Numerical Analysis of Angled IRJs

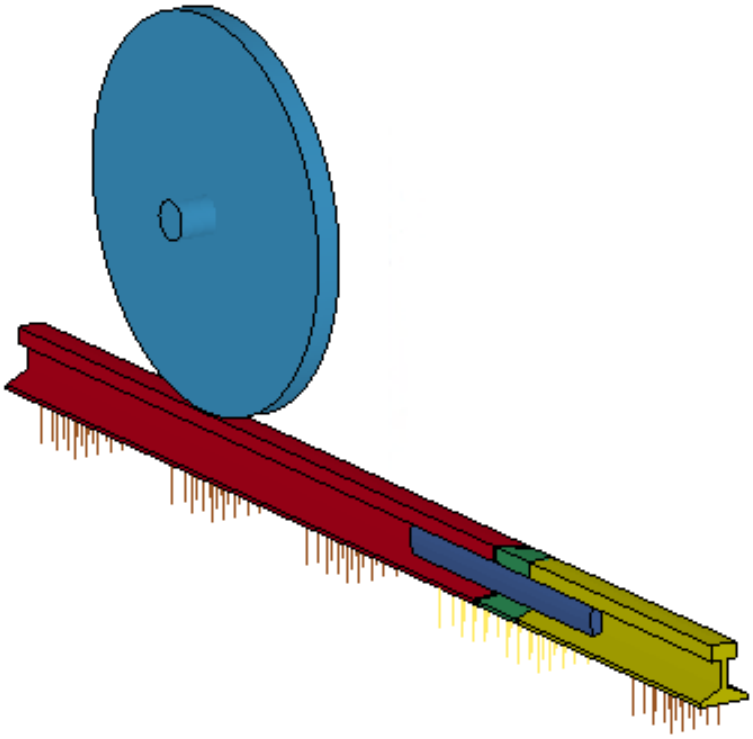

Martin Rijneveld

Delft, 21-02-2021

[page intentionally left blank]

Numerical Analysis of Angled IRJs

By

Martin Peter Rijneveld

A thesis submitted in partial fulfilment of the requirements for the degree of

Master of Science

in

Civil Engineering

Assessment committee:

Prof.dr.ir. Rolf Dollevoet (Chair)

Dr.ir. Zhen Yang (supervisor)

Dr.ir. Pierre Hoogenboom

Dr.ir. Kumar Anupam

Ir. Jelte Bos (Movares)

February 26, 2021

Preface

The master thesis in front of you is quite possibly one of the toughest things I had to do. Especially in the strange situation the world is in right now. I would have never guessed it would have such an impact staying at home. This thesis is a product I am proud of and marks the end of my days as a student at the TU Delft.

My gratitude goes to my daily supervisor Zhen Yang. He kept me going, was always available for a meeting and after our discussions I always had a better view of what I wanted and what I had to do. I would like to thank the others from my graduation committee for the valuable input at the meetings we had. Rolf made sure the scope was clear and the practical use was not forgotten. Jelte provided really helpful information from real-world experiences on railway engineering. Pierre made sure that the project was repeatable and understandable for a wider audience, and Anupam showed some interesting insight coming from road engineering.

A thank you is in place for the ICT-department of the TU Delft, who have restarted the desktops I used countless of times for me.

A big thank you to my family and friends is in order. Supporting me throughout the project and motivating me really helped. The questions you asked me were invaluable and helped me steer the project and keeping the goal in sight. Even the simple request of explaining what the hell I was doing ensured I had to know and understand the subject.
A special thank you to Christiaan for proofreading the report as meticulous as you did.

As a last thing I would like to thank you for reading this thesis and I hope you will learn something from it!

Martin Rijneveld
26-02-2021

Summary

Travelling in a safe, fast and reliable manner is a high desire for many people and countries. For railway travel the Insulated Rail Joint (IRJ) is a critical part in the system, as it is a key part of most railway safety systems but at the same time also considered as a weak link. The IRJ creates a discontinuity in stiffness and geometry that leads to wheel-rail impact forces. This dynamic wheel-rail interaction has been of interest for numerous studies. The angled IRJ is a proposal to reduce these impact forces. It is already manufactured and in use in certain countries, yet also discontinued in other countries. Despite the real-world experiences the research on the topic is marginal.

In this thesis a study is presented into the dynamic behaviour of the wheel-rail impact occurring at IRJs. Numerical models are established to simulate a wheel rolling over IRJs with angles of 0, 15, 30 and 45 degrees using the implicit-explicit sequential finite element method with the software ANSYS/LS-DYNA. The impact forces are the main output and analysed. Three variations of the IRJ models were used for simulations.

The basic version IRJ model is built up with a fully constrained rail foot to simulate an infinite support stiffness condition. The second version is supported by spring and damper elements to simulate supports such as ballast and rail pads. Height differences between the rail ends are generated when a wheel passes the joint, which corresponds to a real-world scenario. Different degrees of support degradation are simulated by varying the support stiffness, using the spring and damper element parameters. The third version also incorporates the spring and damper elements as support but couples some nodes between the fish plate and rail web in vertical displacement to reduce the rail height difference caused by wheel pass-by, aiming to simulate a 'factory-new' condition joint.

The established models were validated in terms of wheel-rail contact solution and contact force amplitude. In comparison with existing FE wheel-rail impact models the proposed models in this thesis are less time consuming and more flexible for joint angle adjustments. The second version simulating degraded joint conditions provided the most interesting findings and was used in a sensitivity analysis by varying the velocity and wheel load.

The simulation results show that angled IRJs are advantageous when degradation is present, whereas in 'new joint' conditions the gap width plays a significant role and angled IRJs with larger gaps produce higher impact forces. Based on the results the recommendation is given to consider angled IRJs on tracks with a low maintenance scheme and further research is suggested.

Table of Contents

Preface 4
Summary 5
1 Introduction 8
1.1 Purpose of an IRJ 9
1.2 Geometry of an IRJ 10
1.3 The Challenges of IRJs 10
1.4 Finite Element Analysis 13
1.5 Scope of this Thesis 13
1.6 Structure of this Thesis 14
2 Previous Research and Angled IRJ use history 15
2.1 Queensland studies 15
2.2 Analysis and field test from urban metro systems 16
2.3 Tapered joint analysis from the U.S. 17
2.4 General conclusions and points of interest from other studies 18
2.5 From manufacturers and the government 20
2.6 Summary of Literature Study 21
3 Theory on angled IRJs 22
3.1 Hertzian contact theory 22
3.2 Gap definitions 22
3.3 Contact area during impact 24
3.4 Summary on IRJ Contact Theory 25
4 Numerical Model Definitions 26
4.1 Attempt to change (Yang et al.,2018) 26
4.2 New Model Simplifications 27
4.3 Model and material properties 29
4.4 Validation and comparison of the newly created model 31
4.5 Simulation output 33
5 FE-Model 1: 'Infinite Support Stiffness' 35
5.1 Model information 36
5.2 Results for different angles 36
6 FE-Model 2: 'Loose Bolt' 39
6.1.1 First results of the three FE-model 2 versions 41
6.1.2 Preliminary discussion of FE-model 2 42
6.1.3 Results from FE-model 2 with all angled IRJs 43
6.2 Discussion of results from FE-Model 2 44

6.2.1 Results with higher support stiffness 45
6.2.2 Discussion of 10/20K results 45
6.3 Conclusions from FE-model 2 46
7 FE-Model 3: 'Factory New' 47
7.1 Results from simulations 48
7.2 Discussion of results 50
8 Discussion of Total Simulation Results 51
8.1 Fixed Nominal Gap 51
8.2 Fixed Longitudinal Gap 51
8.3 Stiffness change 52
9 Sensitivity Research 53
9.1 Wheel Load 53
9.2 Velocity Change 54
10 Concluding remarks 56
10.1 Recommendations 57
11 References 58
Appendix A: Element Descriptions 62
Appendix B: Contact theory in FEM 65

1 Introduction

Railway transport is a mode of transport which can be found almost all over the world. It is a safe, sustainable, and efficient way of moving both goods and people. Railway transport can be done fully electric and gains popularity. The European Commission even declared the year 2021 as 'European Year of Rail' as part of the 'Green Deal' (European Commission, 2020).

In the Netherlands railway operations are very important for the mobility of a lot of citizens. Every day 1.3 million people take the train to travel across the country, but also to other countries. Berlin, Paris and London can all be reached in a single train ride from Amsterdam (Kroeze, 2019).

Figure 1.1: (left) IRJ in Australia at 15 degrees (Mandal,2010); (right) square cut IRJ in the Netherlands (ProRail,2019)

Although accidents still sometimes occur, railway transport is a very safe way of transport. A lot is regulated and every train movement in the Netherlands is directed, similar to the way movements of aircraft are (ProRail, 2020). The most common way of regulating train traffic is done using a piece of rail called the 'Insulated Rail Joint' (IRJ). This is a joint of two rails which are electrically insulated from each other, thus creating sections of rails when multiple IRJs are used. For the Netherlands alone there are about 50 000 (Movares, 2020) of these IRJs installed in the 7000km network (ProRail, 2020).

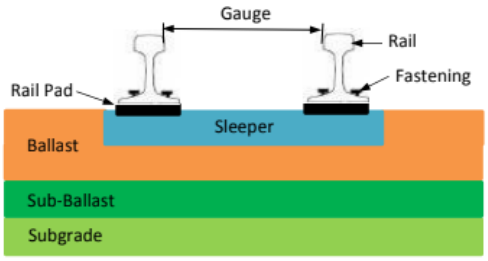

Figure 1.2: Schematic cross section of standard ballasted track (Elshukri, 2016)

Ballasted track is the most common type of track used. The rails are fixed to sleepers with a fastening system. Between the rail foot and the sleeper is a rubber-like rail pad which dampens vibrations and distributes forces. The sleepers are embedded in the ballast, which are small rocks piled together to form a foundation. Underneath the ballast may lay a sand layer, depending on the local ground conditions. In the Netherlands these layers are often necessary. The whole structure is designed such that the high weight and forces from the trains can be resisted without deformations or movements.

Due to the heavy weight of railway vehicles and the use of steel in the wheels and rails the contact dynamics are characterized by high forces and small contact areas. The steel wheels and rail do not deform much in the way a rubber car- or bicycle-tire does. This means that railway travel is very efficient as little energy is lost due to deformations, but it also means the contact area is very small. Combined with the weight of railway vehicles this results in high stresses. The hard steel wheel material also means there is a high sensitivity to geometry changes in the contact area.

1.1 Purpose of an IRJ

IRJs are needed as part of the safety system for railways. Although other systems are available and installed in various countries, the system with IRJs is the most commonly used. It is an old system of which a patent has been found from 1908 (Dalton, 1908), however it is believed to be older than that. Because of its simplicity it is quite robust and reliable and still in use today.
The safety system works via track currents. Each section, defined by IRJs on either side, has a small current running through one rail, via a relay, back to the other rail. This connected relay is thus powered and switches a signal to green or 'clear'. When a train enters this section, it shunts the rail. The current now no longer goes via the relay but through the axle of the train, which is often together with the wheels one piece of conducting steel. The unpowered relay switches the signal to red or 'danger'. If the train leaves the section, the relay is powered again, showing 'clear' for any next oncoming train.
This system is robust as it can also detect rail fracture and is easy to manipulate for track workers to provide a safe workspace. However, it relies heavily on good contact between the rail and the train wheels. Contamination of the rails by for instance leaves can cause the shunting to not work properly. (Rijneveld, 2020)

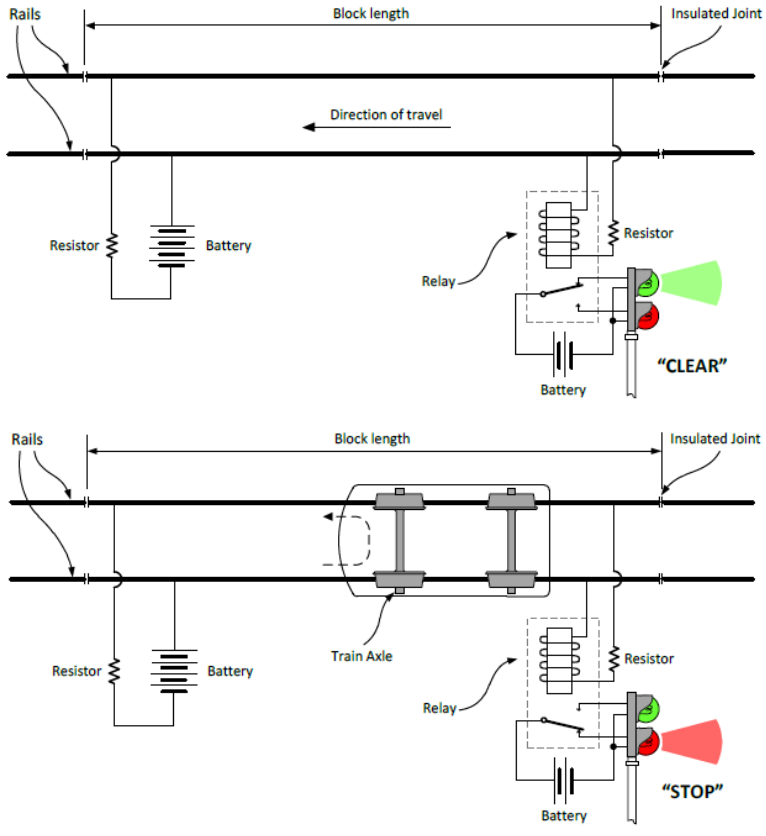

Figure 1.3: safety system using track currents and IRJs (Scalise, 2014)

1.2 Geometry of an IRJ

As explained in the previous section IRJs are an important part of the railway safety system. It consists of two rail ends with a piece of insulation material in between them, called the 'end post', which is often some type of plastic. On the sides of this joint are fish plates, in other literature also referred to as 'joint plates' or 'joint bars'. In between the fish plates and the rail is insulating material, often with glue-like properties. Bolts through the fish plates and rail web tighten everything together. In the Netherlands this IRJ is made at a factory, transported as a whole unit to the trackside and installed on-site using thermite welding to connect to the normal rails.
The end post in the IRJ is the big disadvantage. The stiffness of the end post is practically zero, meaning it will deform much more under the same load than the surrounding steel rails will. The difference is so significant that in most models the end post is 'modelled' by a gap.

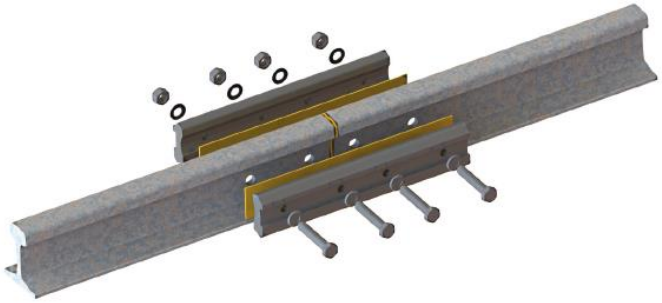

Figure 1.4: The IRJ and the parts it is made of (Quirchmair et al., 2020)

1.3 The Challenges of IRJs

Due to the very low stiffness of the end post and the discontinuity in the rail the IRJ is considered to be one of the weakest links in the railway system. The IRJ also has a lower bending stiffness compared to continuous rail. Although the glue and the fish plates are the parts that provide the IRJ with some stiffness, an IRJ will deflect more than a continuous rail would. The impacts at the IRJ can cause some loud noises that can be heard in the train and can cause noise annoyance in the surrounding area (Bundesamt für Umwelt, 2015).
The IRJ can be an expensive part of the railway system. (Gallou et al., 2018) presented that in the U.S. IRJs can have a life span of 12 to 18 months. (Himebaugh et al., 2008) mentioned IRJ failures in the UK can cost Network Rail around £5 million per year. Figure 1.5 shows that in Austria the IRJ (Isolierstoβ in German) was the cause for 42% of the railway disruptions in 2016, excluding switches.

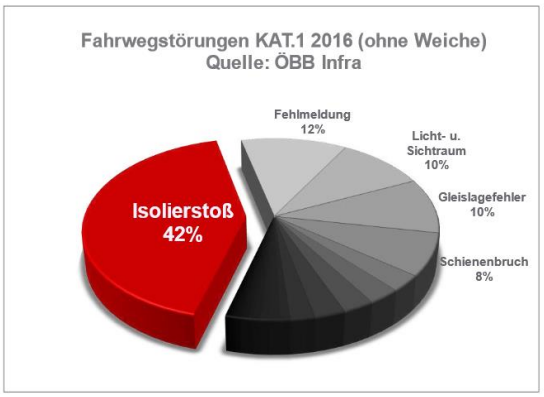

Figure 1.5: Different causes of railway disruptions in Austria in 2016 (ÖBB Infra, 2017)

An important problem is that when an IRJ has a defect, impact forces increase further. These higher forces then speed up the process of degradation, not only on the rails and joint itself, but also of the support structure. This in turn creates even higher impact forces and these effects keep strengthening each other, illustrated in figure 1.6.

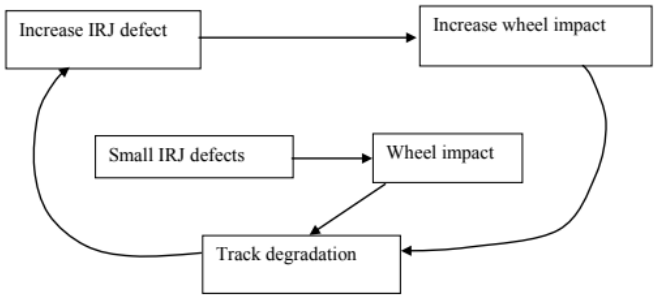

Figure 1.6: Degradation loop of IRJs (Mandal,2010)

(Dhanasekar,2013) reported that the most common failure modes of an IRJ are:

- Bond Failure / delamination of end post
- Broken joint bar / loose bolts
- Failed insulation / metal flow

Bond failure refers to the glue that is used between parts, for instance between the end post and the rail ends. When this occurs the joint and especially the end post can move more freely. Sometimes the end post itself has been degraded down or pushed out of the joint. The delamination and pushing action can also be caused by the high axial forces that can exist in rails. With the continuously welded track most common today the temperature stresses are taken by the rail and the substructure. The gaps formed after delamination (figure 1.7) are often quickly filled with particles which can cause electrical failure. Next to that water can enter the created gaps, which speeds up the gap growth and degradation of the whole joint.

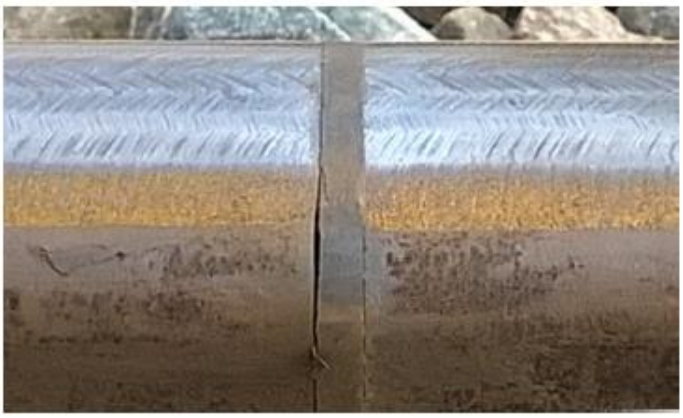

Figure 1.7: Delamination of end post and rail end (J. Bos)

If a joint is not maintained correctly the degradation may cause breaking of certain parts of the joint. Bolts may come loose or cracks form in the fish plates which can lead to fracture. The effect on the joint is that the bending stiffness greatly reduces and a 'dipped joint' occurs where both rail ends bend down. A broken fish plate or loose bolts mean that the two rail ends are not properly connected anymore. This will cause a difference in rail height: as one rail deflects down, the other does not follow. Due to this geometric misalignment such a 'step-up' may cause very high impact forces and double contact situations (figure 1.8).

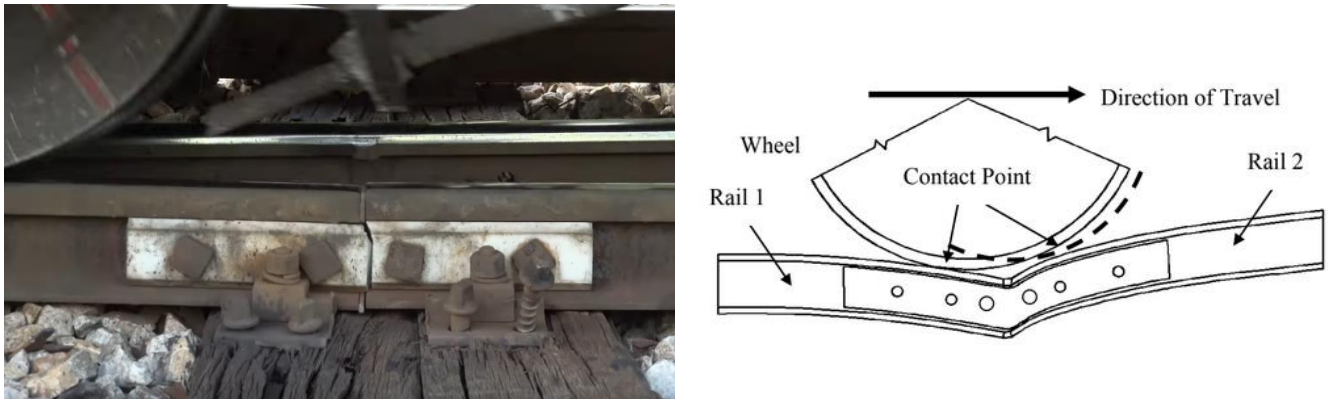

Figure 1.8: (left) Broken fishplate (Youtube); (right) schematic of double contact at dipped rail (Mandal, 2014)

Failure of the insulating layer is often noticed by a functional failure. Apart from faults from the manufacturer or instalment errors it often starts with some deformation or mechanical failure such as delamination. Small particles can accumulate and conduct electricity from one rail to the other. Another reason for failure can be the so-called metal flow or metal yielding. Metal is a ductile material with a yield stress. When the acting stress exceeds the yield stress the material will 'flow' and plastically deform. This happens on the edge of the rail ends, squashing the material and reducing the gap between the two rails. This can lead to an electrical connection and a non-functioning IRJ.

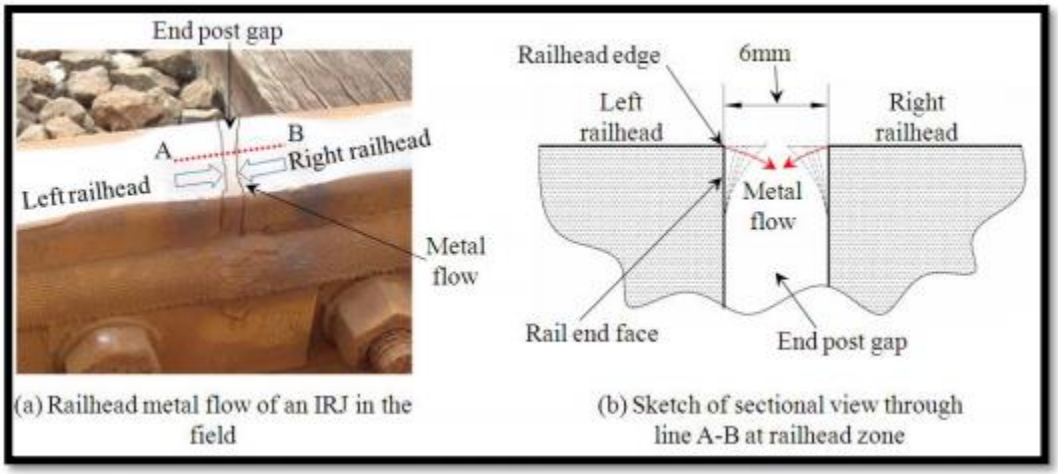

Figure 1.9: Explanation of IRJ failure due to metal flow by (Dhanasekar,2013)

1.4 Finite Element Analysis

The method used for this thesis is Finite Element Modelling, or FEM. This method is used a lot by engineers all over the world as it is flexible and can handle all kinds of situations such as non-linearities, which would be very time-consuming or even impossible with analytical methods. FEM does need to be set up properly and may still produce some strange and unexpected results which need to be thoroughly analysed. Results will not always be the exact truth or show the whole picture.

In FEM the main idea is to divide the structure of interest into a lot of elements, each with their own properties. All these elements can be solved, often with matrix calculation, as each element has properties and boundary conditions. For this thesis both main types of FEM are used: implicit and explicit in a sequential method. The implicit part is a static equilibrium calculation of the wheel on the rail. It does not take into account effects that depend heavily on time, such as inertia. The resulting equilibrium is then the input for the explicit dynamic analysis. Implicit FEM solves directly for displacements and is unconditionally stable, meaning the iteration steps to get to the equilibrium situation can be as large or small as desired. In contrast, the explicit analysis solves the dynamic situation for acceleration, then calculates back to displacements. This analysis takes effects such as inertia into account and move step by step till the end position or specified time is reached. This is *not* unconditionally stable, and the time step should be below a certain threshold, in this case being the time a soundwave can travel through the smallest element. (Yang et al., 2018)

Most settings for the FE-analysis were selected from (Yang et al., 2018) and used in this thesis, as the models in built in this thesis are based on that model. It is however modified to be easily adjustable and shorter in simulation times. More information about element types and other settings can be found in appendix A or in (Yang et al., 2018).

1.5 Scope of this Thesis

In this thesis a study is performed into the possible benefits and drawbacks of angled IRJs. Angled IRJs are regarded as low-impact and thought to outperform normal IRJs (Dhanasekar, 2011). The contact forces between rail and wheel are simulated with FE-modelling software. The difference of peak impact forces between normal and angled IRJs are of interest, with the angle as variable. Other parameters such as wheel load, velocity and support stiffness may be altered as well. The stresses and strains in the wheel and rail itself fall outside the scope of this thesis.
Presented angles are presented in relation to the lateral axis (cross section plane, so perpendicular to the rolling direction) of the rail unless otherwise mentioned. The longitudinal direction aligns with the rolling direction.

1.6 Structure of this Thesis

This thesis report is structured the same way the established FE-model evolved. Chapter 2 dives into the use history of the joint and shows previous research on insulated rail joints. Some information from IRJ manufacturers and an e-mail conversation with a manufacturer employee is summarised. Chapter 3 continues with some contact theory and reasons why the angled IRJ could behave different than square IRJs. Chapter 4 shows the principles and general information about the finite element modelling, and lists the simplifications done to make the model fast and adjustable. Chapters 5, 6 and 7 each consider the difference between angled and standard IRJs, but in different situations and constrains. They handle fully constrained rail foot (infinite support stiffness), rail height difference ('loose bolt' IRJ) and 'factory new' situations respectively. After that chapter 8 looks into the effect of velocity and wheel load change in the 'loose bolt' situation. Chapter 9 discusses the simulation results of all models and compares them. In the end chapter 10 presents some concluding remarks and recommendations on further research and when to apply an angled IRJ.

2 Previous Research and Angled IRJ use history

As the IRJ is considered by many to be one of the weakest links in the railway system the IRJ has been extensively researched. Field test measurements, lab specimen testing and numerical simulation analyses can be found about the IRJ and the various parts it consists of such as the end post, glue material or fish plate shape and length. Almost all literature found related to standard square cut joints. Interestingly the angled joint is already in use and in some places has also already fallen out of favour again, but research done on angled IRJs seems to be lacking. The lack of research was also mentioned by (Dhanasekar, 2011), which is a paper from a larger research project in Australia into the IRJ and included a small part about angled joints. Next to this project a few other studies have been found relating (in part) to angled (or inclined) IRJs. A short summary of the found studies is presented.

2.1 Queensland studies

This large research project in Australia (Dhanasekar, 2013) provided a good understanding of IRJ behaviour. The final report consisted of a few papers and reports and summarised it. This final report gave a general overview, so some of the results presented here are from the original papers itself as these were more detailed.
Some interesting facts that followed from report:

- The associated annual cost for maintenance and repair of IRJs is estimated at $5.4million direct and $1.1million indirect;
- The width of the end post in Australia may vary between 5mm to 10mm;
- Reduction of impact forces should be done via gap size/end post width reduction;
- Track modulus modifications such as support stiffness are less productive in impact force reduction than geometric modifications;
- Ratchetting and metal flow are the main failure mode, mainly due to the stiffness difference and the sharp rail edge;
- From 2005 onwards predominantly 15-degree joints are manufactured;
- The gap size/end post width has been restricted to 4-6mm in 2007, where 8-10mm was not uncommon before.

(Mandal,2010) was a paper incorporated in the larger research project. It provided a general insight in IRJs. A basic model was made for FE analysis. The width of the end post was 10mm, modelled with epoxy fibre-glass material from *table [1].* The sleepers were modelled using fully constrained nodes, and full connection between fish plate and rail was done via coupling of node deformations. A 180kN load was applied in the middle of the joint. The dynamic load factor (or impact ratio) ranged between 1.05 and 2.45, and the model generated short duration P1- and long duration P2-forces.

Table 1: End Post material properties used in (Mandal,2010)

Materials	Young's Modulus, E (MPa)	Poisson's ratio, υ
Epoxy fibre-glass	4500	0.19
Nylon 66	1590	0.39
PTFE	400	0.46

(Mandal, 2013) used an FE model to assess damage if the end post had come loose or was not glued to the rail ends. Both 5mm and 10mm gaps are considered, using a peak vertical pressure load of 2500MPa applied at one rail end. This pressure was taken from a dynamic factor of 1.16 and a wheel load of 174kN. No numerical values were shown for the used stiffness or damping.

A paper close to the study presented in this thesis was (Dhanasekar, 2011). In *Performance of square and inclined insulated rail joints based on field strain measurements* the author acknowledges that there was a lack of literature covering angled joints, although these are in use in Australia and claimed to outperform square IRJs. A hypothesis is made that the angled IRJ will endure more shear due to eccentricity, but that the impact duration is shorter but higher for square joints.
Strains measured in field testing showed that the vertical strains were smaller, but the variability higher for the angled joint. Bending and shear strains appeared lowest for the square joint.
However, no general conclusion on the difference between angled and square IRJs was presented because only one specimen was tested, and for a much shorter time than initially planned.

(Askarinejad, 2016) is a paper which formulated a new explicit multi-body dynamic model incorporating detailed wagon, wheel-rail subsystems and track containing a rail discontinuity (i.e., a rail joint). The predictions of the localised track responses were validated using the data from two gapped rail joints in a field test. Measured strains were converted to forces and resulted in an impact ratio of 1.34 to 1.7. In the semi-analytical model the fish plates were fixed to the rail web, all sub-systems simplified in one layer of springs and dampers and the gap modelled with one element of negligible stiffness.
Sensitivity analysis on the gap size showed that a larger gap causes a significant rise in wheel-rail dynamic force. However, the rail deflections seemed to increase only marginally with the increase in joint gap size.

2.2 Analysis and field test from urban metro systems

(El-Sayed et al, 2018) is a comprehensive study into the mechanical and electrical deterioration of IRJs. An elastic-plastic finite element analysis was used using ABAQUS, with stresses and strains in the IRJ contact area as main results. The model had the end post modelled with 4500MPa stiffness, but no glue layer, fish plates or sub-structure as only the response of rail material was of interest. The end post gap was 8mm, the used load 110kN and a wheel diameter of 510mm.
A few parameters were investigated, all with the aim of reducing ratcheting and increasing service life. Just as (Dhanasekar, 2011) the square or rounded rail ends were investigated. Angled joints were also considered. They concluded that at an angle of 5 degrees (or 85 degrees if measured from longitudinal axis; see angle α in figure 2.1) the peak stresses reduce the most and there was 20% less metal flow. Larger angles such as 15 and 30 degrees had a reduction of stresses that was less significant, but all seemed to reduce the metal flow.

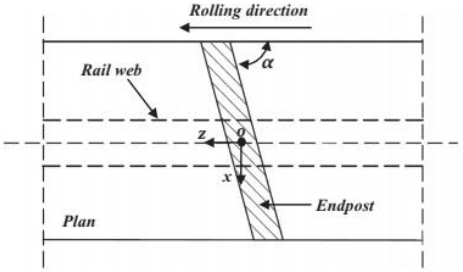

Figure 2.1: Angled joint from (El-Sayed et al, 2018)

A field measurement study was performed on the Terhran-karaj urban metro system by (Ataei et al, 2016). The noise and displacements of sleepers near the IRJs were measured, where the IRJs were square, 30- and 45-degree versions (measured from the lateral rail axis). They found that the 45-degree joint had less sleeper displacement than the 30-degree joint, and both were less than the 0-degree joint. Acceleration signatures of these sleepers were almost half compared to square joints. A final observation was that the 30-degree joint generated the least noise, which is often associated with impact forces.

2.3 Tapered joint analysis from the U.S.

An investigation in the U.S. by (Plaut et al,2007) was done on tapered joints, seen in figure 2.2. A tapered joint is an angled or inclined joint with the ends rounded off up to the 90-degrees again. In terms of contact mechanics these are equal to angled IRJs, but the mechanical and axial behaviour can differ. The service life of IRJs in the U.S. can be as short as 12 months, and the tapered glued rail joints should provide some advantages over conventional insulated rail joints, such as lower deflections, bending moments and shear stresses in the adhesive. Both an analytical and an FE-analysis were done, although properties from the FE-model were unclear.
At least two simulations were done with angles of 8 and 2.4 degrees. Bolts were modelled as forces and the glue layer with an elastic material. Sleepers are modelled by placing select regions of elastic foundations.
In comparison with a conventional insulated butt joint, the tapered joint showed to exhibit smaller values of maximum deflection, bending moment in the rails and joint bars, and shear stress within the adhesive.

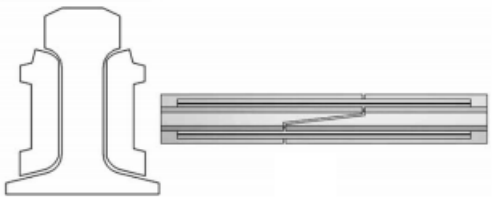

Figure 2.2: Tapered IRJ considered in (Plaut et al,2007)

(Akhtar,2007) showed that the lap joint (tapered joint) had excessive chipping of railhead material on the running surface, but also showed 60% less maximum stresses compared to standard joints using a static FE analysis. The lap joint also showed about 15% less strains. The end post was modelled as a gap.

(Himebaugh, 2008) refers to these American studies and from another study (which could not be found for analysis) that determined that the best design of a tapered joint would have a length of at least 8 in. (roughly 200mm), with an optimal length of 27 in.(685mm) and an angle of about 2 degrees. This design would yield lower stresses in the epoxy layer. The study itself considered the way the epoxy layer and the rails interact.

Figure 2.3: Long tapered test joint from (Akhtar,2007)

2.4 General conclusions and points of interest from other studies

From the numerous reports and research done on IRJs a couple mention angled joints or draw conclusions based on papers that were not found. Some information about gap width and numerical values for stiffness and impact ratio were searched for to compare with values used in the study in this thesis.

In the Netherlands in 2002 some research was done on new insulated joints (RailInfrabeheer,2002). Alongside the normal square joints also inclined and 'V-shaped joints were tested. These joints failed the axial force tests, probably because the rail foot was also cut at an angle. It was found that there was more pollution in the joints.

(Cai et al., 2007) modelled a joint with height difference between the rail ends, which significantly affects the contact force, stresses and strains. The coupled ANSYS/LS-DYNA implicit-explicit FE-method was used to simulate different rail end height differences, wheel loads and velocities. The gap used was 8mm, and all substructure elements like ballast and rail pads were combined in a single spring/damper element ($K = 3.09 \cdot 10_7$ N/m, $C = 1.44 \cdot 10_4$ N s/m). They found (near) linear relationships with the impact force and both velocity and height difference, and results indicated that train velocity difference had more effect than axle load difference.

(Zong,2013) looked at the rail end, which with the square sharp corners induces high impact forces and stresses. These can get extreme values due to the singularity of a sharp corner. A more optimal rounded corner provided higher impact forces, but significantly reduced stress levels when simulated in FEM.

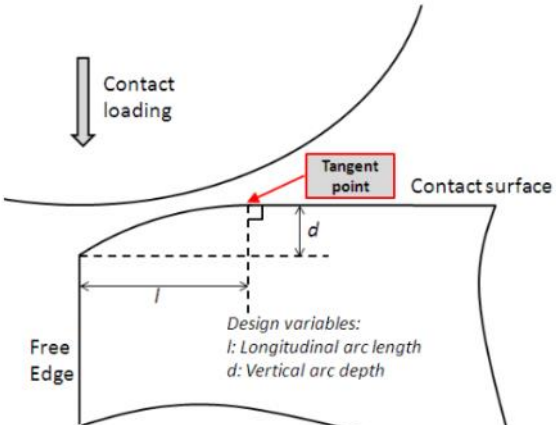

Figure 2.4: Rounded rail edge from (Zong, 2013)

Although the angled IRJ may be regarded as a new concept, the study '*Innovative Design Concepts for Insulated Joints'* (Charlton,2007) did not mention angled IRJs at all, apart from a quick reference to (Plaut et al,2007).

An interesting conflicting reference is in (Németh et al., 2020), where a first reference to (El-Sayed et al, 2018) mentions the benefits of non-perpendicular joints such as reduced vertical deflection. Later however a reference to a not to be found study [*Insulated rail joints assembled with high strength bolts*], by the '*ÖBB Infrastuktur'* (Austrian infrastructure manager) stated that the inclined joints are not more suitable or appropriate based on railway operator's practice.

(van Dyck et al,2016) did a study into the impact ratio (or dynamic factor) and the use for it in design principles. With rising axle loads the existing methods in the U.S. needed an update. Figure 2.5 shows the design values for the dynamic load factor used by various organisations, with the velocity changing at a 0-degree IRJ. For 100km/h (around 60mph) the factor ranges between 1.2 and 1.6.

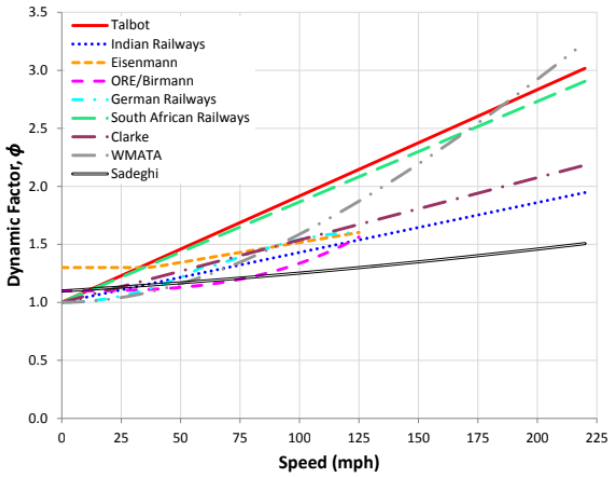

Figure 2.5: Dynamic factors (Impact ratio) depending on velocity, used as design parameter by various organisations (van Dyck et al,2016)

(Gallou et al,2018) states that the dominant failure modes of rail joints in the UK are insulation (29%) and fishplate failures (23%). It used FEA to study the structural deflection of rail joints under a static test with fatigue inducing load. An impact ratio (dynamic factor) of 1.6 was used.

A PHD thesis by (Yang, 2018) reported a model of a standard square cut IRJ in the Netherlands using the implicit-explicit sequential finite element method. It is a model which uses spring/damper elements to simulate ballast, rail pad and fastening systems together with fully modelled sleepers. A wheel with normal profile on half axle is loaded with sprung masses to simulate the bogey and car body. Outputs of the model are displacements and forces, but also vibrations and stresses. The model is validated using comprehensive field measurements of a wheel pass-by and a hammer test. It showed good agreements of the contact area simulated and measured running band.

2.5 From manufacturers and the government

The angled joint is already in use, and some companies can be found online that advertise them. In Europe there are two large manufacturers of rails and attributes such as IRJs and switches, namely 'Vossloh' and 'Voestalpine'. Both of them have a location in Germany and supply among others to the German infrastructure manager 'DN Netz' and the Dutch equivalent 'ProRail'. These manufacturers both make and advertise the 30-degree angled IRJ and as far as could be found not any other angles, although on demand production is likely to be possible.
The designs of both manufacturers are nearly identical. At 30 degrees the railhead is cut with some rounding off at the side edges. The rail web and foot are still cut at 90 degrees to enable the joint to handle large normal forces with less shear forces due to the angle.

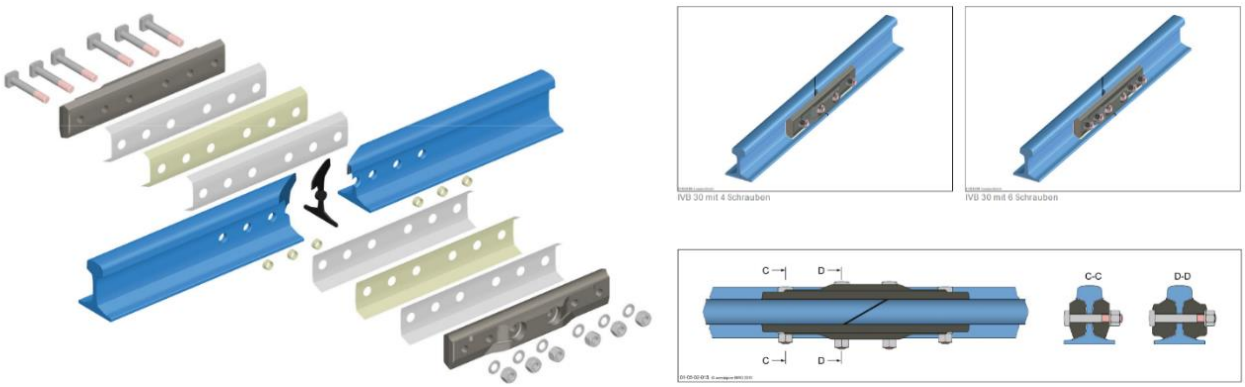

Figure 2.6: angled IRJ from product flyer (Voestalpine GmbH, n.d.)

Voestalpine claims that their 30-degree IRJ 'makes it possible for the wheel to pass smoothly without abrupt interruptions' (voestalpine,n.d.). Furthermore, compared to standard IRJs an angled IRJ should be more resistant to wear and have a lower noise level as far as the wheel transfer area is concerned. Alongside these benefits the angled IRJ would have a deflection comparable to continuous rail and does not require extensive maintenance. With all these benefits it is expected to find this type of joint very often. Also some intensive research done on this topic would be expected.

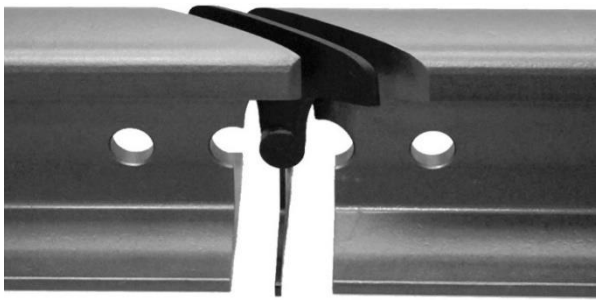

Figure 2.7: Angled IRJ from (Vossloh AG, n.d.)

The other main manufacturer 'Vossloh' also mentions that the 30-degree IRJ has an 'impact-free transition between rails, allowing noise reduction, less wear and extended life cycles' (Vossloh AG, n.d.). It is also brought up that this type of joint is the standard insulated joint in Deutsche Bahn regulations. However, after e-mail conversations with a Vossloh-employee it turns out that in 2016 the regulations changed back in favour of the old 90-degree IRJ. On questions why the reply mentioned that there was too much defects were occurring at the joints. More information could not be found, even after more e-mails to the manufacturers and DB-Netz. In the same conversation the employee did mention that Denmark (Banedanmark) and the United Kingdom (Network Rail) were planning to or are already using the 30-degree joint.

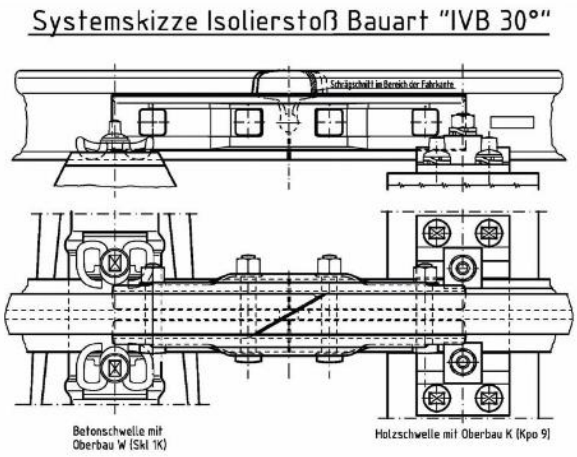

Figure 2.8: Schematic drawing if angled IRJ (DB Training & Bahn, 2016)

From governments and infrastructure managers not a lot of information could be found. Next to the single e-mail reply the official notice that the 30-degree IRJ is allowed can be seen. On 23-09-2009 the angled IRJ is admitted (Eisenbahn-Bundesamt,2009), and in 2015 this was extended (Eisenbahn-Bundesamt,2015). However, this extension was until 10-2019, so it seems that indeed in Germany the now favourite IRJ is the 90-degree model again.

The requirements in the Netherlands state that the gap in the IRJ, or the thickness of the end post, should be at least 2mm with a maximum of 8mm. It seems however that most new joints are installed with a gap of 6mm, although it can differ. In Australia joints with thicknesses ranging from 6mm to 15mm are used (Dhanasekar, 2013).

2.6 Summary of Literature Study

The existing literature shows that the angled IRJ is being used and remarkably already abandoned too. Despite the apparent experiences and opinions on the subject the research is minimal. it may well be that there is more research done but this is confidential or not digitalized. A few studies compared real-world data between angled and standard IRJs which showed that the angled IRJ deflects less in vertical direction but endures more shear stresses. Using a FE-Model the deflections have been studied, however not impact forces or stresses on varying angles of IRJ.
The study in this thesis aims to fill the gap.

3 Theory on angled IRJs

A first look into the angled IRJs is a theoretical approach. Investigating existing theory on contact mechanics between objects may help in predicting if an angled IRJ will perform with less impact forces. Gap definitions are used to distinguish certain situations and an attempt to explain the impact dynamics at square and angled IRJs from (Dhanasekar, 2013) is shown.

3.1 Hertzian contact theory

The wheel-rail interface is a contact mechanics problem. A long time ago (Hertz, 1882) developed a theory on the contact area, and stresses within that area, for two bodies in contact. This theory assumes full elasticity and no friction conditions, which are not fully fulfilled in real-world wheel-rail contact. It can still produce a good estimate which is used by al lot of other researchers to validate their models and is used for the study in this thesis as well.

The Hertzian contact theory uses the radii of the separate bodies in contact and converts them to two mathematically equal bodies, of which the contact area and stresses can be calculated. The theory itself can be found in (Hertz,1882).

The contact solution of two bodies such as a wheel and rail has a circular or oval shape, with two principal radii. The contact stress is highest in the middle and the edge of the contact area. This is illustrated in figure 3.1, with O-a and O-b the radii of the contact patch and Pm the maximum stress. It should be noted that this is a solution of non-rolling wheel. In the situation of a rolling wheel other aspects such as tangential stresses play a role as well, but for the total contact force this is not significant. A comparison of the Hertzian solution and the FE model used in this thesis can be found in chapter 4.3.

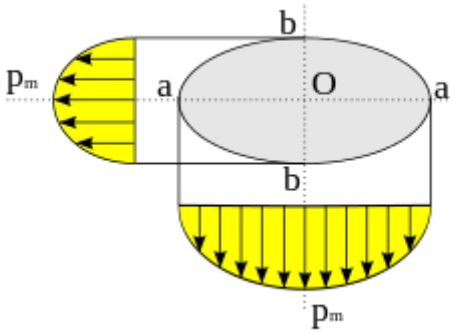

Figure 3.1: General contact solution from Hertzian contact theory (Wikipedia.nl)

3.2 Gap definitions

There are regulations on every part of the railway system, thus also for IRJs. These are however quite hard to find. The requirements found cover a lot about the insulating threshold and the axial forces it should be able to resist. A minimum width between the rail end can be demanded as well. None of the requirements found included angled IRJs.

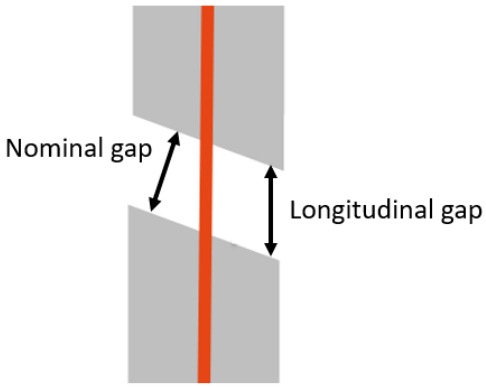

Figure 3.2: definitions of distances

If the requirements would state that a minimum nominal distance is required between the rails then an angle will create a bigger longitudinal gap. This is illustrated in figure 3.2. In this thesis most of the simulations are first performed with a specified width in the nominal direction. With the nominal distance staying at the level from the requirements, the longitudinal distance will change with the angle according to equation 1. Larger gaps are often concluded to result in larger impact forces, meaning the angled IRJ has a big disadvantage with these requirements.

$$L = \frac{d}{\cos(\alpha)} \qquad \textit{Equation (1)}$$

$L = Longitudinal\ gap$
$d = nominal\ gap\ width$
$\alpha = angle\ of\ IRJ\ measured\ from\ lateral\ axis$

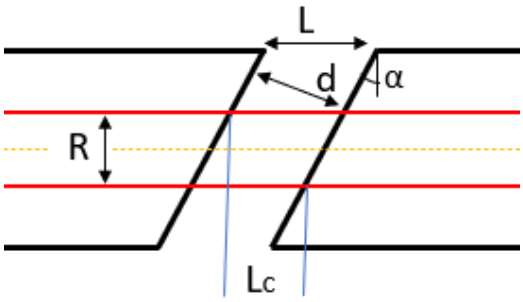

Figure 3.3: Gap geometry of an angled IRJ

However, equation 1 does not take the contact width into account. As figure 3.3 indicates, due to the angling the longitudinal distance between the last contact point of the first rail and the first contact of the second rail can decrease. Although wheel-rail contact areas are considered very small there is still some width, which will negate the longitudinal distance slightly. Expressed in analytical terms this is equation 2.

$$Lc = \frac{d}{\cos(\alpha)} - 2 * R * \tan(\alpha) \qquad \textit{Equation (2)}$$

$Lc = Longitudinal\ crossing\ gap$
$d = nominal\ gap\ width$
$\alpha = angle\ of\ IRJ\ measured\ from\ lateral\ axis$
$R = Lateral\ width\ of\ contact\ area$

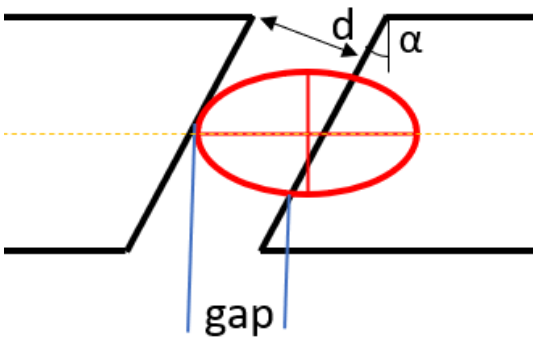

Figure 3.4: Gap geometry of an angled IRJ and oval contact patch

When the oval shape of a contact patch is considered the gap between the two points of contact will look like figure 3.4. The actual distance is depenent on the oval shape, which in turn is dependent on rail and wheel geometry and wheel load. With the shape in figure 3.4 the actual gap would have a value between the resulting values of equation 1 and equation 2.

3.3 Contact area during impact

The contact patch has a circular or oval shape, and the highest stresses are in the middle (Hertz,1882). The green bar and triangle in figure 3.5 show the contact area increase on rail 2 during the time in which the wheel has 'landed' on rail 2 with the widest points of the contact patch (red oval) and the time it fully disconnects from rail 1 (green dotted oval).

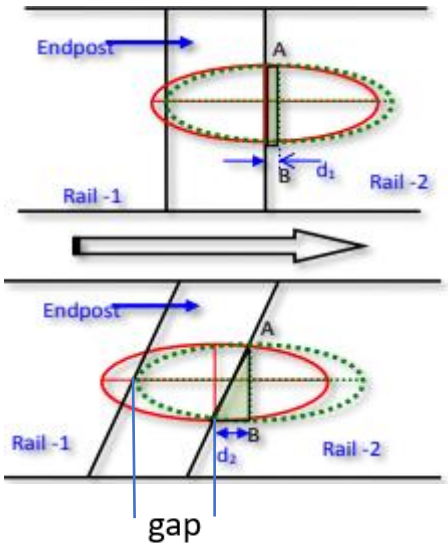

Figure 3.5: schematic visualisation of contact area at IRJ impact, square vs. angled joint (adapted from (Dhanasekar, 2011))

It is assumed that the impact force occurs when the middle axis of the shown contact area (which is where the highest contact stress is) 'lands' on rail 2. The velocity and material properties are equal between rail ends and between the standard and angled IRJ. Figure 3.2 then shows that the impact duration of an angled IRJ is longer, which can lead to lower peak impact stresses (Dhanasekar, 2011). It also shows that the angled IRJ takes the impact with an eccentricity, which may result in a different stress distribution compared to standard IRJs. This is however outside the scope of this study.

3.4 Summary on IRJ Contact Theory

Depending on the gap requirements the angled IRJ has a big disadvantage that the distance between the two rail ends in longitudinal direction is increased if the angle is increased. A larger gap is often considered to result in higher impact forces. When the width of the contact patch is considered this gap reduces slightly. However, as the contact area is small so is the distance reduction.
It is also possible that there is no requirement on the nominal gap and the longitudinal gap can remain the same between the square and angled IRJ. In that case there is no gap difference and no direct impact force difference due to tis gap difference.
(Dhanasekar, 2011) showed that a square IRJ endures a shorter impact which is expected to result in higher impact forces than the angled IRJ. It should be mentioned that all figures in this chapter assume no height difference between the rail ends and show a 2D scenario.

4 Numerical Model Definitions

In this chapter the used FE-model is explained. Simplifications and important parameters such as material properties are presented and a comparison with Hertzian contact solutions is performed.

4.1 Attempt to change (Yang et al.,2018)

At first it was tried to simulate different angled IRJs by using the model from (Yang et al.,2018) and adapt it. This model is a sophisticated sequential implicit-explicit FE model which is calibrated to a specific square IRJ in the Netherlands. The model can reproduce the vibrations and wave patterns created when a train passes the joint while it can also show the contact stresses and contact area. The model has a UIC54 rail modelled (used in the Dutch network), complete with sleepers and spring/damper elements for the ballast, fastening system and rail pads. A wheel with part of the axle and mass elements representing the car body and bogey are also modelled. More detailed information about the model and its algorithm can be found in (Yang et al.,2018).
(Yang et al., 2018) is thus very detailed, but that also means it the simulation times are long, reaching 20 hours depending on computer hardware properties. An attempt was made to only change the IRJ to an angled IRJ of 30 degrees. Due to the detailed and complex geometry of the rail, standard volume-cutting techniques of the software used did not work and resulted in a lot of errors for inconsistencies and discontinuities. A solution can be to use less precise elements (tri-angular instead of hexahedral), or to divide the rail in more separate parts and build it out of smaller pieces. When the second option is implemented the modelling work is not finished, as the spring dampers from the rail pad and fastening system should be reattached at exactly the right places. Creating nodes to attach to at these places while still maintaining a well distributed mesh would take a lot of time.

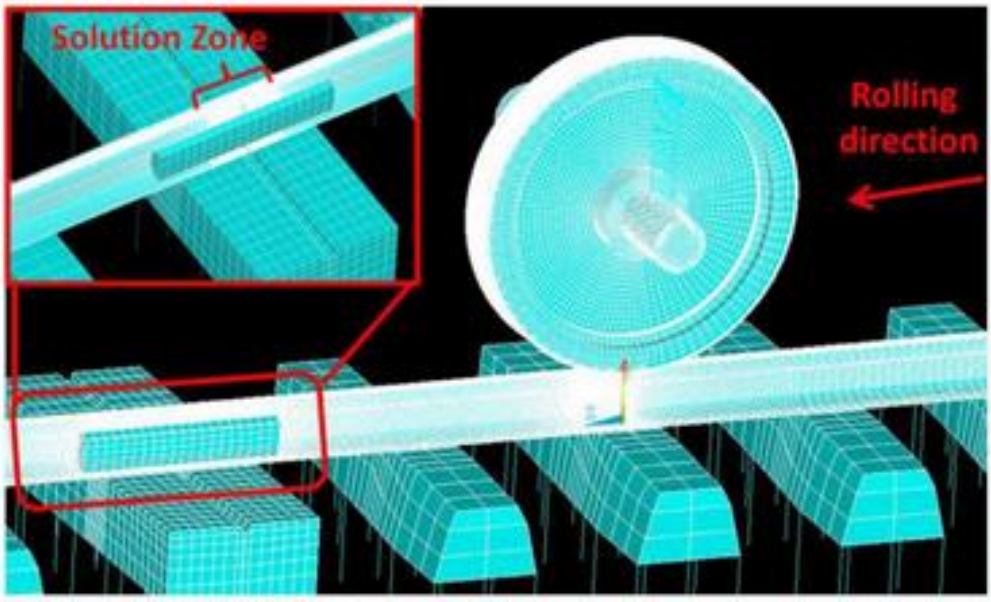

Figure 4.1: The model from (Yang et al., 2018)

To get to know the modelling software and the analysis procedure a very simple and basic model was created. In this simple model the wheel was only a cylinder and the rail a half-circle, shown in figure 4.2. Because changing the elaborate model was found to be slow and time-consuming, combined with the initial aim to try a few different angles and designs, an attempt was made to create a new model. It is based on (Yang et al., 2018) and uses the same method, software settings and algorithm.

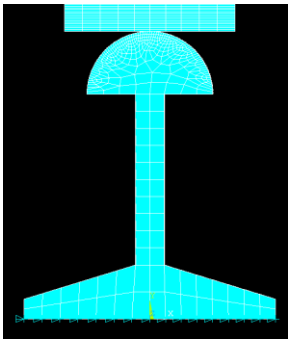

Figure 4.2: very basic rail cross section

4.2 New Model Simplifications

The newly established model is simplified compared to (Yang et al., 2018) in order to make it suitable for easy adjustments of the IRJ and faster simulations. The most important simplifications and the assumptions accompanying them are now presented, together with the argumentation.

Rail Design

One of the main reasons for creating a simplified model is the detailed rail profile in the original model which causes introducing changes to it quite time consuming. Instead a new cross section is proposed which has the same radius on top at the running surface while the rest of the cross section is less detailed. As Hertzian Theory showed, the radius of the body in contact heavily influences the contact area and the contact stresses. Therefore using the same radius on top of the rail should result in a comparable simulation result as (Yang et al. 2018).

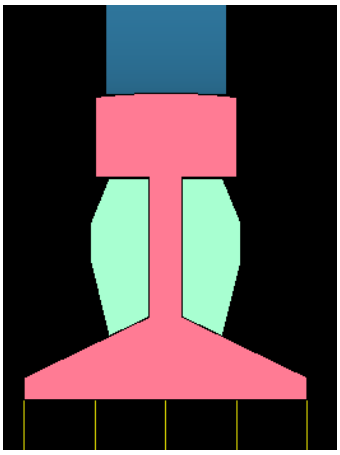

The overall shape and dimensions such as height and width are the same, so the actual beam properties should not differ. The deformation will then also be comparable.
The mesh of this rail is fine at the contact area and coarse at the rest of the volume, following the method from the original model. This study focusses on the contact force and not the vibrations induced on the rail. Therefore, the mesh is less dense for the whole model. In order to gain good results for contact force and contact area, some test simulations were conducted and results were compared with the original model.

Figure 4.3: Cross section of rail and fish plates

Wheel

Changes to the wheel profile are similar compared to the changes to the rail profile. The wheel is modelled with less elements and only a fine mesh is used at the outer rim, where there will be contact with the rail. Figure 4.7 shows a part of the meshed wheel.

Sleepers

No sleepers are present in the new model. It is assumed that the sleeper itself moves as a rigid body with little deformation and damping in the material. The presence of sleepers would however mean that the rail will more or less deform as a straight part over the width of the sleeper. To simulate this behaviour the lowest nodes of the rail are coupled together in vertical deformation, such that these are constrained together, creating sleeper-like behaviour.

Fastening system and substructure

In the original model the rail pads and the fastening system are modelled using spring and damper elements at precise locations. In the newly established model these elements are partially incorporated, depending on the model version. The stiffness and damping of these elements in vertical direction are modelled using one spring, together with the stiffness and damping of the ballast. In lateral direction the new model is fully constrained. It is assumed this motion does not heavily influence the contact force.

Car body and bogey

To accurately model the effects of the bogey and car body and their inertial contribution they are modelled in (Yang et al., 2018) with special mass elements (see appendix A for the element descriptions). These elements are set on spring and damper elements, modelling the various suspension parts between the train and the wheel.

This system is simplified by applying a force directly on the middle nodes of the axle. This way the force can be more easily altered. A direct force instead of moving sprung masses is also faster in simulation times. The force is applied on all middle nodes of the axle to prevent large deformations in the axle. This does not affect the force distribution at the wheel-rail surface using the principle of (de Saint-venant,1882). The axle can also be shorter and this saves elements for shorter simulation times. The reduction in elements was not that significant.

Mesh and number of elements

Due to the new cross sections for wheel and rail, the absence of sleepers and the combination of some spring and damper elements the total amount of elements is significantly lower in the newly established model in this thesis. This will have a positive effect on the simulation time, suiting the model better for parameter changes. However, a too coarse mesh will eventually lead to loss of accuracy. When not enough elements are present the deformations of the nodes become too large and the model may produce inaccurate results and singularities.

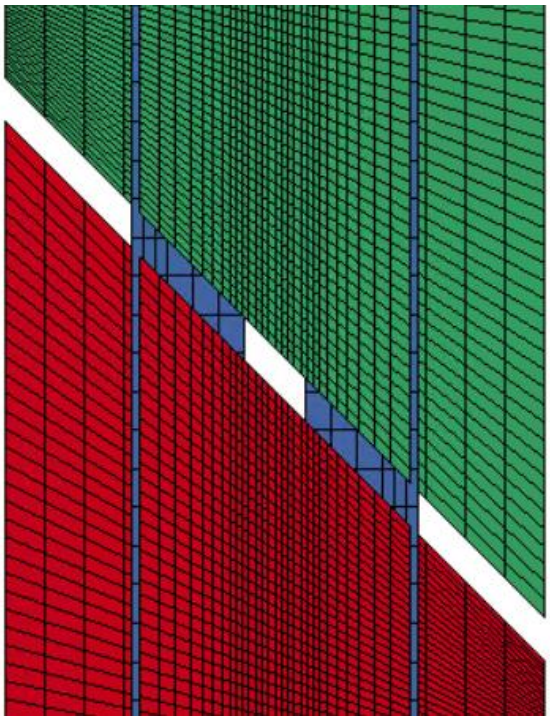

Figure 4.4: Top view of 45-degree joint with rail 1 (red), rail 2 (green) and fish plates (Blue)

4.3 Model and material properties

Due to the simplifications mentioned in the previous section such as the combining of stiffness and damping of certain parts the material properties need to be changed and are shown in table 2. All rigid bodies (wheel, rail and fish plates) are simulated with the properties of steel. The material is modelled as a linear isotropic material for the implicit simulation. In the explicit simulation the steel is modelled with a bi-linear isotropic material.

The substructure is modelled using spring (stiffness) and damper (damping) elements representing the rail pads, sleeper, fastening system and ballast. These elements had to get equivalent stiffness and damping values such that the model is accurate. These equivalent values were calculated using equation 3, which shows the combination of serial springs stiffnesses. The stiffness parameter 'K' can be replaced with damping parameter 'C'. Therefore, obtaining the equivalent value for damping uses an identical procedure. This technique was also used by (Prakoso,2012), (Cai et al., 2007) and others.

$$\frac{1}{Ke} = \frac{1}{K1} + \frac{1}{K2} + \frac{1}{K3}(+\,etc.) \qquad \textit{Equation (3)}$$

Ke=equivalent stiffness

$K1,2,3$=various stiffness values of combined parts

The original values were taken from (Yang et al., 2018). These were combined using equation 3, but slightly altered afterwards. If only one spring and damper element was used per sleeper position, the attached node could get very large deformations. Therefore, under each sleeper a total of 15 spring and damper elements were placed. As these elements are placed in parallel the equivalent value obtained from equation 3 can simply be divided by 15 to get the material property per element, presented in table 2. It shows that the different sleepers used in (Yang et al., 2018) are still present: two wooden sleepers under the IRJ and concrete sleepers under the continuous rail.

Table 2: Material properties

	Stiffness per element [N/m]	Damping per element [N*s/m]	Stiffness total sleeper [N/m]	Damping total sleeper [N*s/m]
Concrete sleeper position	2.44E6	5.57E4	3.66E7	8.36E5
Wooden sleeper position	1.79E6	1.97E4	1.48E7	2.96E5

	Yield strength [GPa]	Poisson ratio [-]	Density [kg/m^3]
Steel	210	0.3	7800

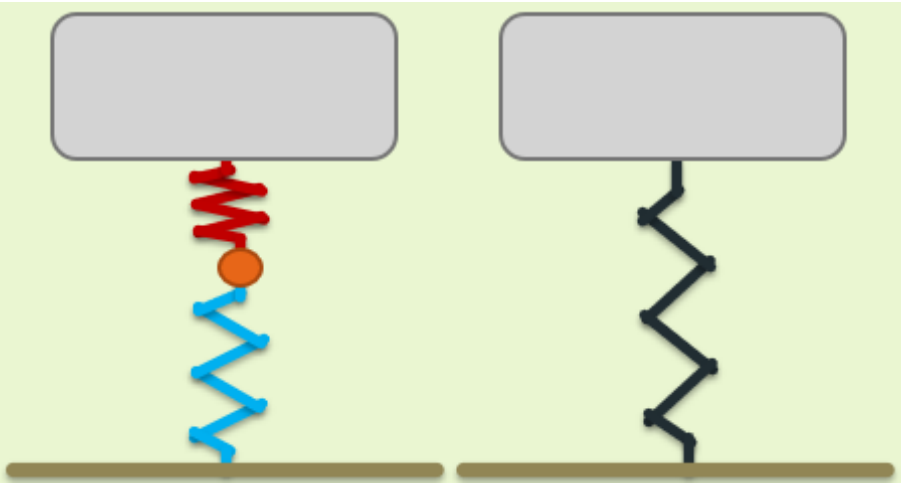

Figure 4.5: Schematic visual of combining spring- (or damper) elements. left shows (Yang et al.,2018) with the dot as sleeper, right shows the simplification from this thesis

Geometrical properties of interest are of course the angled rail end, varying from 0 to 45 degrees measured from the lateral axis. The gap width modelled is 8mm and the wheel on top has a radius of 460mm. The force on the axle is divided over 41 nodes with each a downwards load of 2200N. This results in a force of 90.2kN in total and is used in each simulation, unless otherwise specified.

Constraints are different for the implicit and explicit analysis. In the implicit part the wheel only moves down to an equilibrium situation on the rail. Therefore the sides of the wheel and axle are constrained in all horizontal directions (X and Z), allowing only vertical displacement (Y). this can be seen in figure 4.6. The rail foot is also constrained in all horizontal directions and supported in the vertical direction by the spring/damper elements which attach to fully constrained fixed nodes. For the explicit simulation the wheel is free of the constraint in longitudinal direction (Z) to enable the rolling over the joint. In all simulations the lateral displacement is constrained.

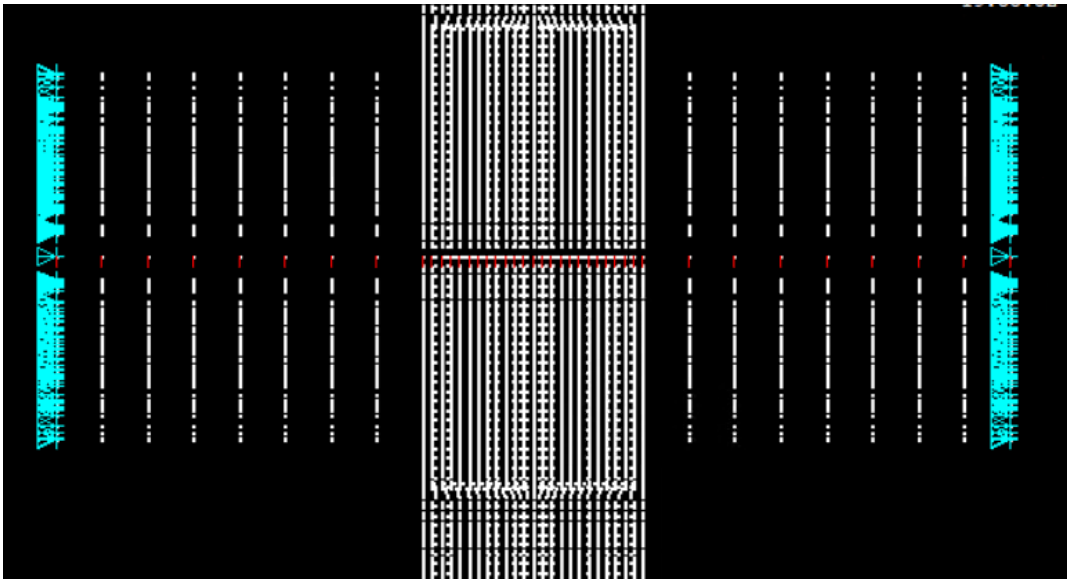

Figure 4.6: Front nodal view of wheel at axle height, with constraints on edges

It should be noted that in the FE-models presented in this thesis the rail is cut over the full height, also when the cut is at an angle. In actual cases most manufacturers showed (Chapter 2) that only the rail head is cut at an angle, but the rail foot is still cut square. This is done to maintain the ability to endure the axial forces which can be present in a rail. As this thesis looks at the contact force the contact area is of main concern, which is the rail head, and therefore it is not significant which way the rail foot is cut. For modelling purposes, it was faster to cut the rail foot at an angle as well.

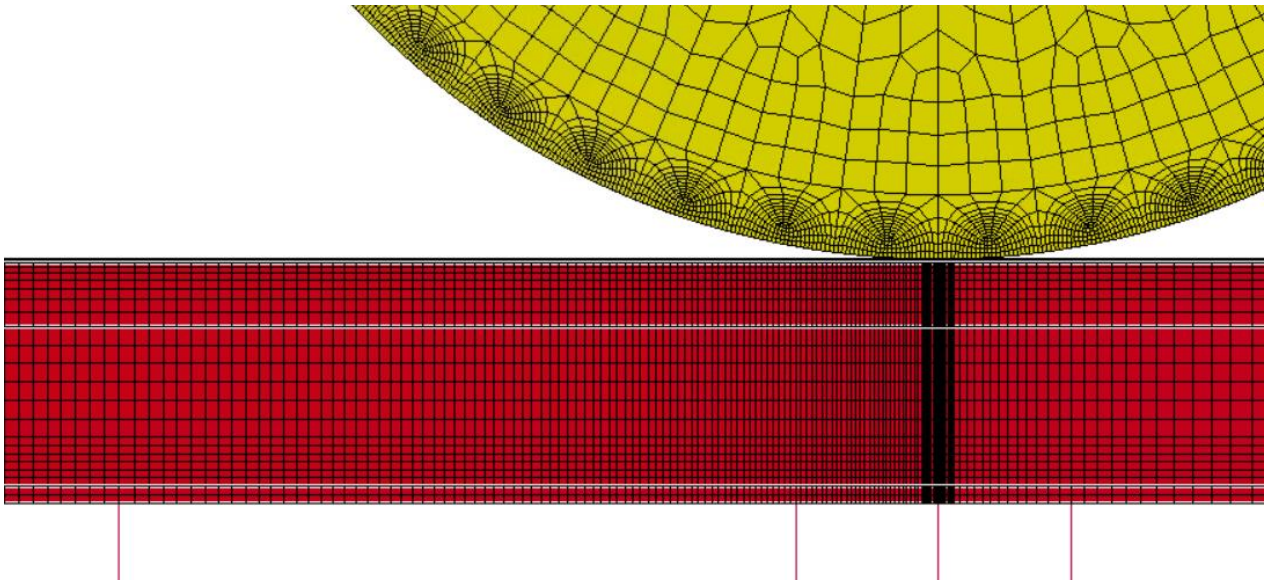

Figure 4.7: Meshed wheel on rail1, showing the mesh used on rail and wheel

4.4 Validation and comparison of the newly created model

The new model is investigated to see if it is accurate enough in terms of contact force. For this a short Matlab-script was used together with an online contact calculating tool (Van Beek,1999…). The first step is to see if the mesh adjustments lead to inaccurate results. Variations in mesh were simulated in the implicit part only. With a very fine mesh the accuracy goes up at the cost of simulation time, whereas with too little elements the contact patch becomes inaccurate and the stress values not accurate anymore. The simulation results using a fine mesh contact solution and the selected mesh contact solution can be checked by comparing them to both the original validated model (Yang et al.,2018a) and Hertzian Theory.

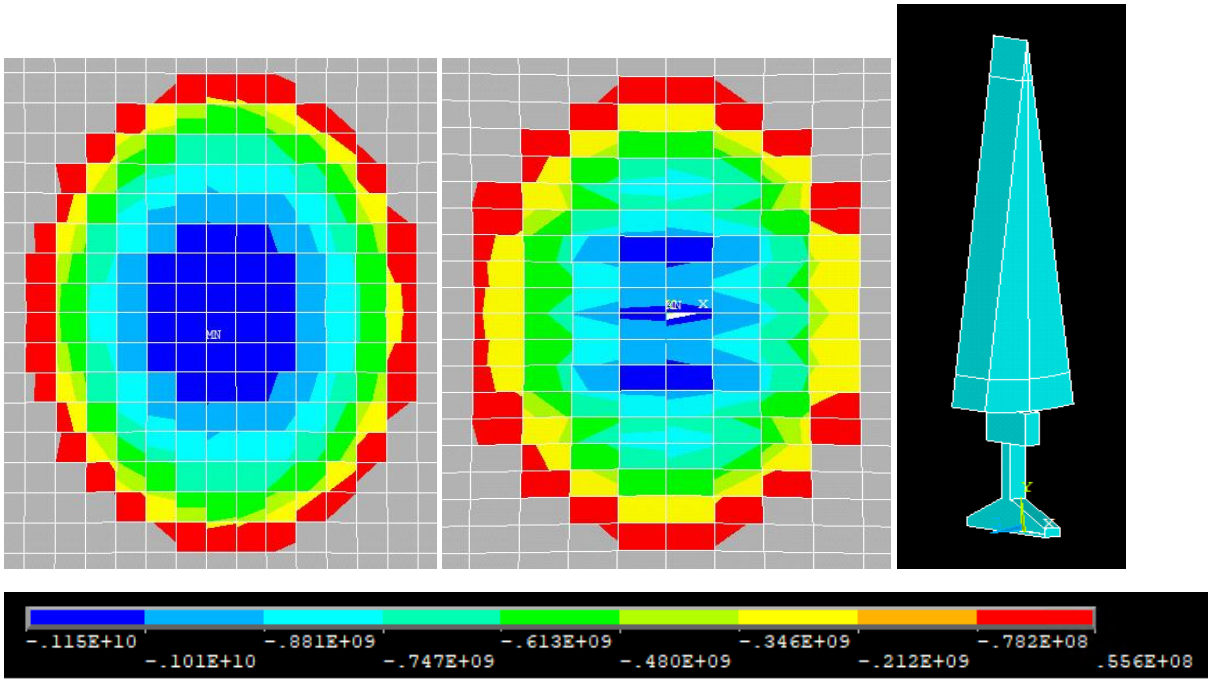

*Figure 4.8: Contact area from differently meshed models, with below a scale [Pa]; (left) a fine mesh of 1mm*1mm; (middle) a coarser mesh of 2mm* 1mm; (right) part of wheel and rail to test the mesh*

To test the mesh, only a part of the wheel and rail were modelled. These modelled parts and the results of the fine and selected mesh are shown in figure 4.8. The coarser mesh that was selected does show less detail and a less smooth colour (stress) transition. The difference in maximum contact pressure with the prediction from Hertzian theory was 11%, with the simplified FE-model being lower. The Hertzian prediction was calculated with a fairly simple Matlab script using two steel cylinders (210Gpa, Poisson ratio: 0.3, radii body 1: 300mm and infinite, radii body 3: infinite and 460mm). The comparison also showed that the contact area from the selected coarser mesh is a bit too large compared to Hertzian theory, which explains the lower maximum stress. Results show that both contact patch radii were around 9% longer than Hertzian contact theory predicted.

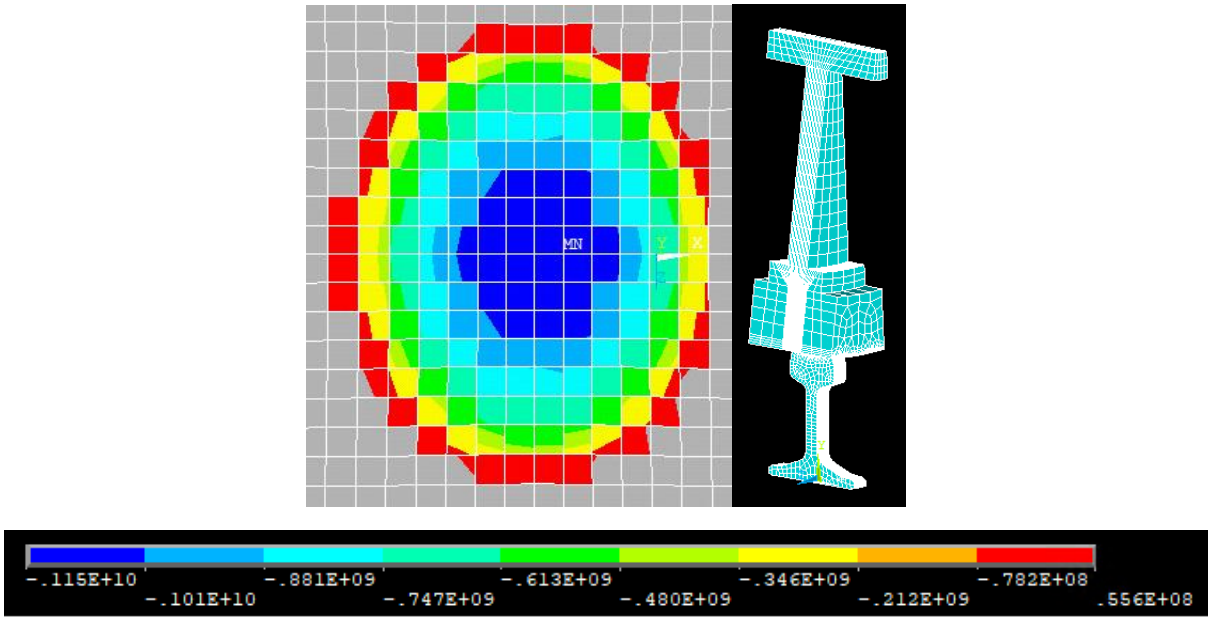

Figure 4.9: Contact patch from (Yang et al., 2018a) adjusted for mesh test. Scale in [Pa]

In comparison to (Yang et al., 2018a) the selected coarser mesh showed the maximum stress was 0.108E10 N/mm^2, which is about 5% lower. The contact patch radii were slightly larger. Figure 4.9 shows the contact area and stresses resulting from (Yang et al., 2018a) with the same loading and algorithm as in this thesis. All presented contact patches in figure 4.8 and 4.9 are very similar in terms of shape, area and stresses. The differences between this thesis' simplified model using the coarse mesh compared to both the well validated (Yang et al., 2018a) and Hertzian contact theory is acceptable. The results from the explicit simulations show that the contact force stabilizes quite fast. The explicit simulation starts with the results of the implicit simulation, so a well transferred force with good contact definitions indicates that the selected coarse mesh does not result in significant errors.

4.5 Simulation output

When the simulations are performed they output different kind of results. First the equilibrium result from the implicit simulation is used as a starting point in the explicit simulation. It is also used to validate that the contact area is accurate enough, as mentioned in the previous section. The results from the explicit simulation are the acceleration of all the nodes at every timestep. This acceleration can be converted to velocity and displacement, which can be used to calculate strains and stresses. Combining the stress and the contact area results in the contact force, which is the result most used in this thesis.

As there are two rails in contact with the wheel over time the result of one simulation are two contact force graphs. These can be seen in Figure 4.11(left), where the green line shows the contact force while the wheel is rolling over the first rail and the yellow line when the wheel starts contact with the second rail after the IRJ gap. Adding these two lines creates the blue graph in Figure 4.11 (right), showing the contact force over the two rails in the entire simulation.

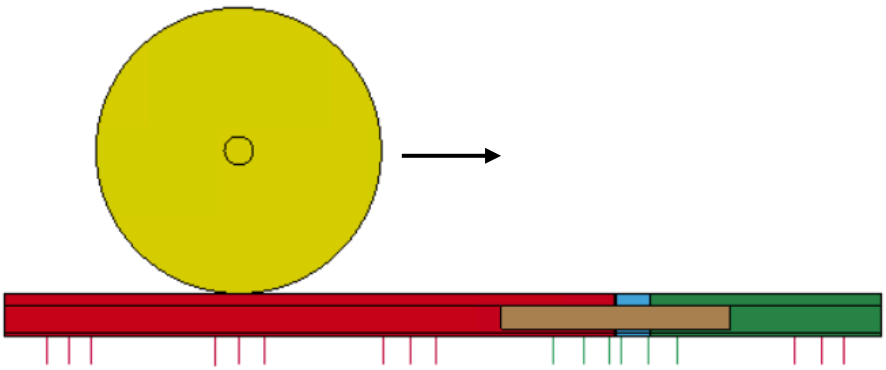

Figure 4.10: visualisation of FE-model.

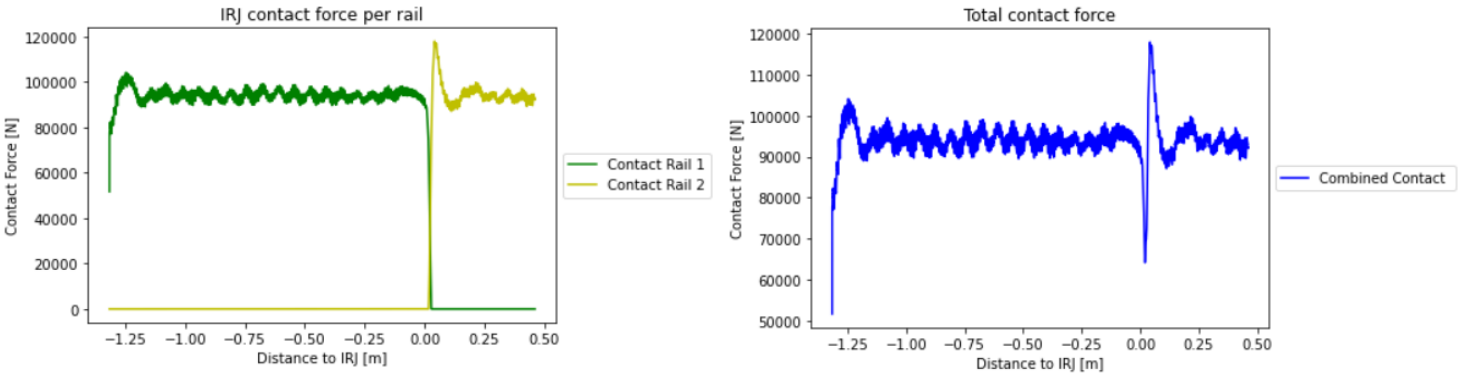

Figure 4.11: (left) contact force of the wheel per rail; (right) Contact forces per rail combined in one line.

In most literature available on IRJs and wheel-rail impact contact mechanics another method of presenting results is introduced, using the impact ratio or dynamic factor. This is the contact force divided by the static or applied wheel load, thus giving an indication of how high the dynamic force is. Most of the time the impact ratio is between 0.8 and 1.2 (Chapter 2). Upon impacting the IRJ (or another geometrical irregularity) the impact ratio can be as high as 3. A new or well maintained IRJ results in a ratio between 1.3 and 1.6. Especially in the case of wheel load change is the impact ratio of interest. The impact ratio also enables an easier and better way to compare with other research when validating the new FE-models.

5 FE-Model 1: 'Infinite Support Stiffness'

The first FE-Model built and simulated is a simple version. With the rail foot fully constrained and not able to move in any direction the sub-structures such as ballast and rail pads are not yet simulated. Thus there is no elasticity or damping. The simulation time needed was very short considering the model still is similar to (Yang et al., 2018). It took around 1 minute for the implicit part and 4-5 hours for the explicit part, instead of 2 hours and 16-20 hours respectively.

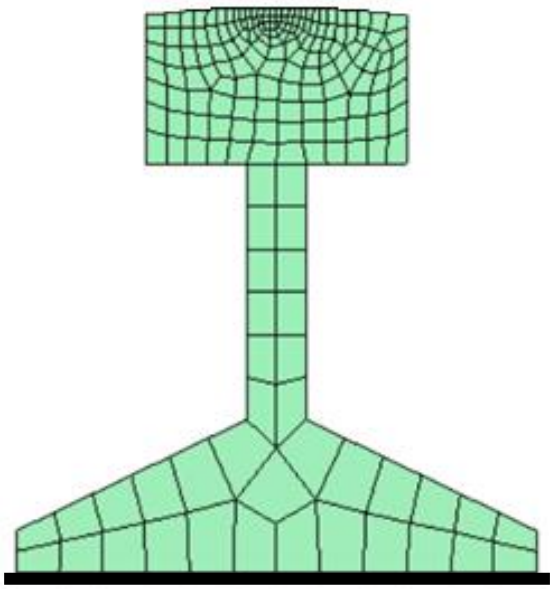

Figure 5.1: Cross section of rail with visible mesh

5.1 Model information

This first FE-model is the most simplified version. In the model the mesh is as discussed in chapter 4, but the spring and damper elements underneath the rail are eliminated. Instead, the lowest nodes of the rail are fully constrained. In other words, the rail can only deform and not translate or rotate in any direction. The material itself has some damping, but compared to the rail pads or ballast it is negligible.

The first simulation done was on a normal (0-degree) square joint. The wheel load was 85kN, simulating a light commuter train, with a velocity of 100km/h. The resulting contact force plotted over the distance to the IRJ of this first simulation can be seen in figure 5.2.

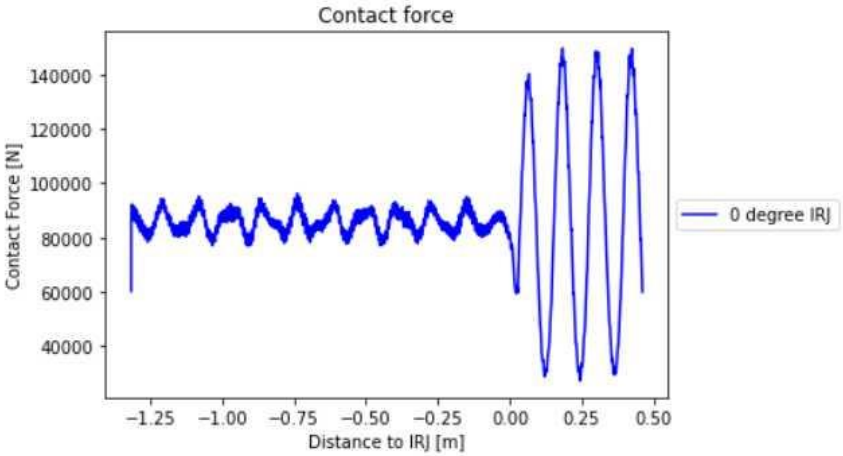

Figure 5.2: Contact force from FE-model 1, 0-degree IRJ

Figure 5.2 shows that the model is fairly stable quickly as the part from -1.3 to -0.1 meters is steady around the applied wheel load. There are some dynamic effects that cause the contact force to vary between 75kN and 95kN. This is expected to be mainly due to the lack of damping elements. The average remains at the right level which is the applied static wheel load. The place of the IRJ is also clearly visible, it is the location where the contact force drops before peaking high. The oscillations after that are due to the fact there are no damping elements in the model.

5.2 Results for different angles

Although the lack of support elements means this FE model is simplified too much to simulate ballasted track it is still used to simulate the angled IRJs for the study in this thesis. Real-world situations which this FE-model could resemble would be an embedded rail where the damping material has completely worn out or a joint encased in concrete. Although not likely to be found in the field the results can show interesting outcomes to base further models on.

The effect of damping is not significant on the first peak, therefore for comparison with other IRJ designs focussing on this first peak can still provide reliable results. Three variants of the IRJ were constructed and simulated at 15, 30 and 45 degrees. The nominal gap is the same for these angled IRJs and the standard IRJ.

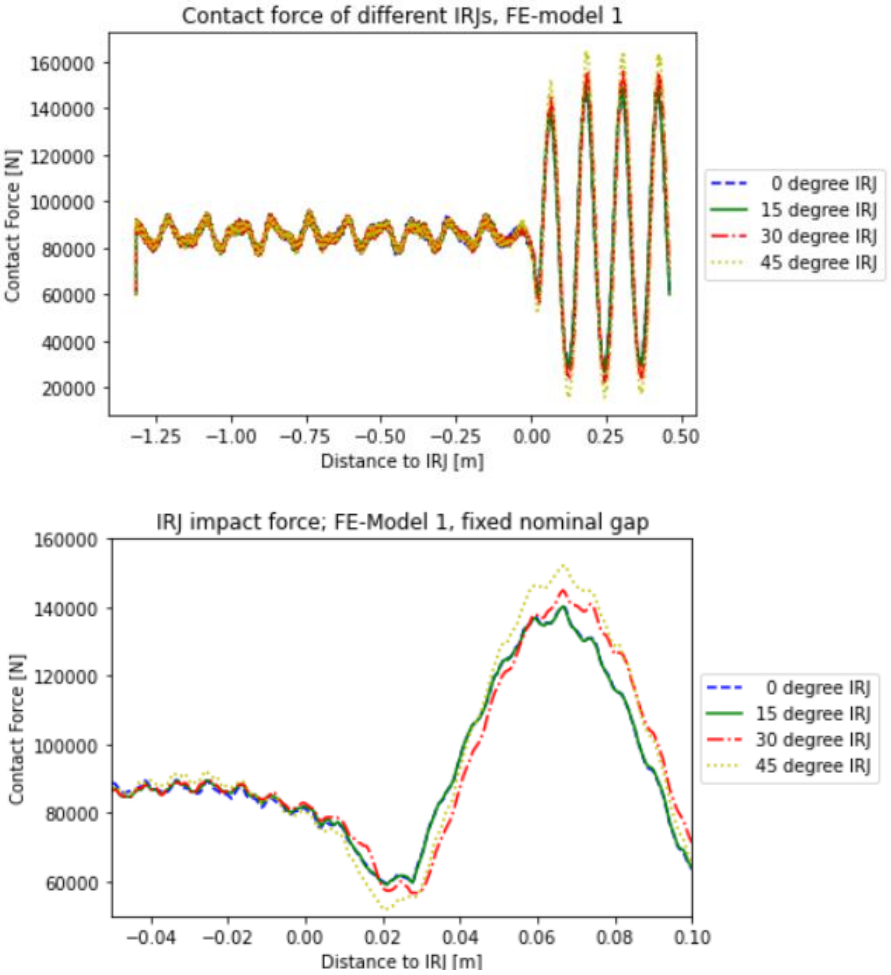

Figure 5.3: Contact forces of FE-Model 1; 0, 15, 30, 45 degree IRJ
(upper) for total duration of simulation
(lower) zoomed in around IRJ zone

In Figure 5.3 the resulting contact force at four different angled IRJs are plotted for the complete simulation, and a zoomed in view of the most interesting part is presented. This is the dip before impact and the first peak after the wheel impacts the second rail. It shows that at larger angles the contact force dips more before peaking higher. The main reason for higher impact forces at larger angles is expected to be the nominal gap staying the same and the longitudinal gap getting larger. This is true for the 30- and 45 degree IRJs, but the 15 degree IRJ is nearly identical to the 0 degree IRJ. Since the results looked identical a check was done to see if the simulations were performing as they should. With a zoomed in view it showed that the 15 degree IRJ did cause a really small difference which was negligible.

When the simulations were performed with the longitudinal gap fixed at 8mm, the contact forces show a similar pattern overall, see figure 5.4. However, in these simulations the results shows no difference in the first impact amplitude. Different graphs can be distinguished at the dip in contact force, so the simulations are in fact separate and different, but do result in the same peak force. The 0-degree joint does dip a bit lower than the angled IRJs.

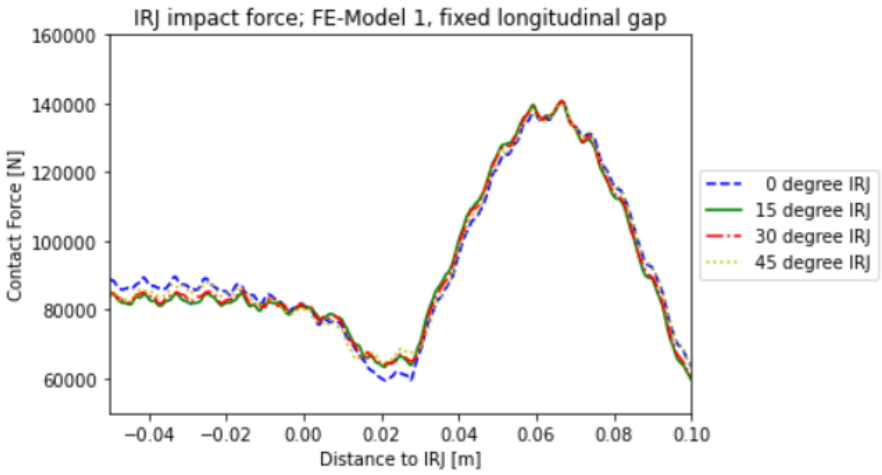

Figure 5.4: Contact force FE-model 1; 0, 15, 30, 45 degree IRJ; 8mm longitudinal gap fixed

Instead of comparing the contact force, the peak contact force can also be expressed using the impact ratio. These are plotted for every angle in Figure 5.5. The four simulations of 0, 15, 30 and 45 degrees confirm that at larger angles the impact gets higher. The impact ratio of the 45-degree IRJ is about 12% higher than the standard square IRJ. The results show that the difference in impact ratio increases, which can be explained with the increase of longitudinal gap using trigonometry presented in chapter 3. The gap is directly related to the cosine of the angle. Compared to the static force plotted in figure 5.4 the amount of extra force due to the velocity and dynamic behaviour can be observed.
For the simulations with a fixed longitudinal gap the impact ratio stays near flat, indicating that there is indeed no significant difference. The change is with -0.5% practically negligible and confirms that the gap distance plays a major role in the impact force.

Chapter 2 summarised that the impact ratio caused by new joint is expected to be between 1.2 to 1.6. This simplified model overestimates the impact force, especially considering that due to the fully constrained lower nodes of the rail, the running surfaces of both rails will be at practically equal heights. In other words, this model simulates factory-new profiles with no step-up between the two rails. A low impact ratio is therefore expected. It should be noted that the spring and damper elements play a large role in the impact force amplitude and are not taken into account in this FE-model 1. Another version in chapter 6 has the spring and damper elements incorporated.

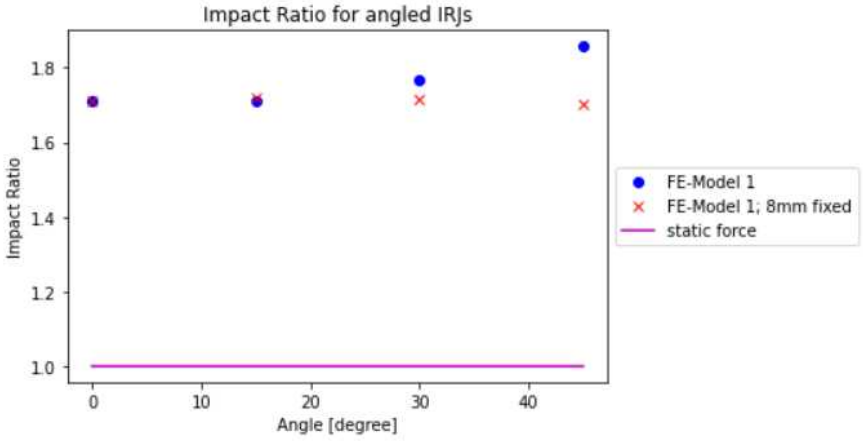

Figure 5.5: Impact ratios per angled IRJ

6 FE-Model 2: 'Loose Bolt'

After the basic FE-model 1 it was decided that the fully constrained rail foot was a too large simplification. This second model is more in line with (Yang et al., 2018) and others, but still has some simplifications. The rail and wheel geometry are more basic and no different from FE-model 1, as is the use of forces on the axle instead of sprung mass elements. The big difference is the use of spring and damper elements to simulate rail pads, sleepers and ballast. Initially the nominal gap is at 8mm for this model. All simulations in this chapter are performed with a velocity of 100km/h and a wheel load of 90kN.

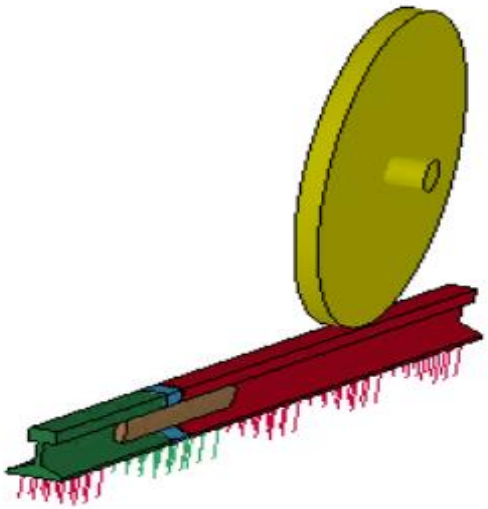

Figure 6.1: Visualisation of FE-Model 2 with visible spring/damper elements in the sleeper positions

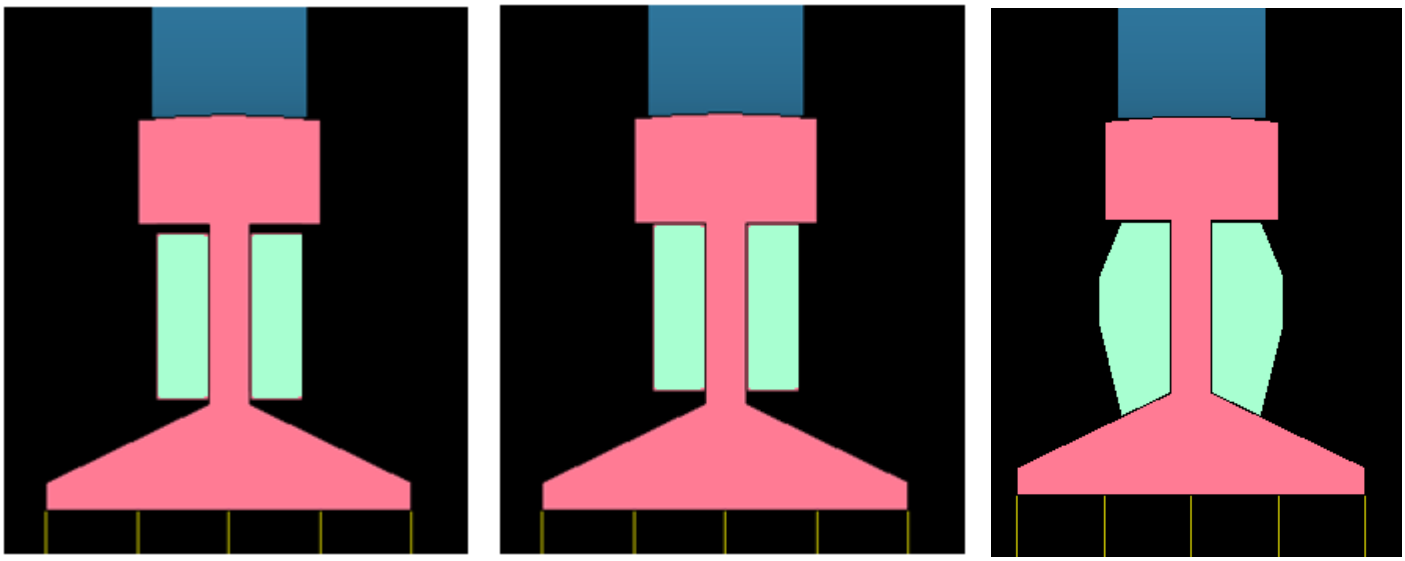

Figure 6.2: Cross sections of FE-model 2; three types of fish plates

There was some evolution in FE-model 2 after the results of the first simulations came in. Due to the new spring and damper elements under the rail foot, the lowest nodes of this rail foot no longer had full constraints. Instead, the nodes were unconstrained in the vertical direction. Therefore the two rails were able to move independently, creating the need for fishplates (also called joint bars or side bars) to be modelled. These plates attached to the side of the rail web are used in the real world as well, in different shapes and sizes. The function of fish plates is to reduce the free movement of the rail ends and provide some bending stiffness to the IRJ. The shape, size and placement of these plates have a large impact on the contact forces. A new fishplate eliminates the difference in height displacement between the rails. In other words, if rail 1 has a downward displacement due to the wheel loading the fish plate forces rail 2 down as well.
After the first simulation of FE-model 2.1 the impact ratio was much higher than in FE-model 1. The impact ratio was high compared to the range mentioned in chapter 2. On closer inspection the fishplate did not touch the railhead and allowed for some slip between the rail, which created the possibility of relative height difference. For a second version (FE-model 2.2) the fishplates were placed higher up. This version still had too much slip, resulting in quite some height difference.

A third version (FE-model 2.3) no longer used a very basic fish plate, but a more modern, full height and wider fish plate. The height difference should reduce enough to get in an acceptable range in terms of impact ratio. This FE-model 2.3 version is more in line with what is expected for this type of simulation based on the existing literature (chapter 2).

The insulating glue layer between different parts of the joint is not modelled in the FE-models in this thesis. (Papaioannou, 2018) reported that this does not have a significant influence on the contact force. Other reports like (Németh et al., 2020) also did not take this layer in account.

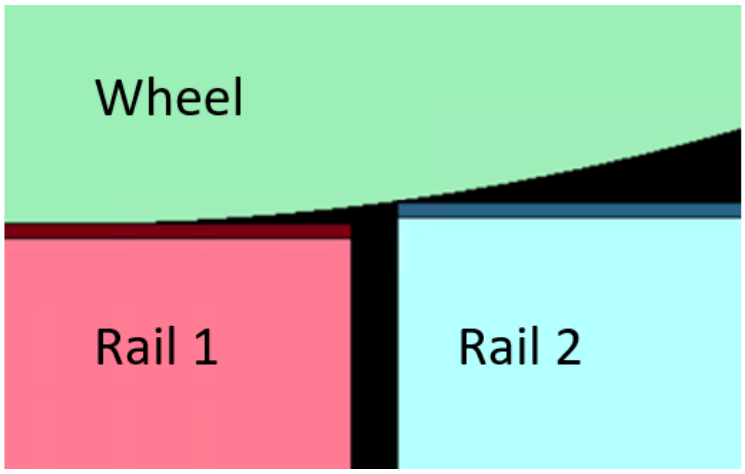

Figure 6.3: Close up of IRJ with visible rail height difference

6.1.1 First results of the three FE-model 2 versions

The resulting contact force of FE-models 2.1, 2.2 and 2.3 are plotted in figure 6.4. Each version simulated a standard square IRJ and a 30 degree IRJ. All three figures have the same axes and scale to allow for better comparison. It is clearly visible that by adjusting the fish plate and its location the peak impact force is reduced drastically. This is visible for the 0 degree IRJ, however the 30 degree IRJ does not change that much.

As mentioned a big contrast with the results of FE-model 1 is the clear presence of damping, visible by the notable lower amplitudes after the first peak. There are no large amplitude oscillations after the IRJ anymore. The second difference in results is the lack of contact force drop before the impact. The contact force instantly peaks instead of decreasing first.

Another interesting finding is that the second impact wave does not change as significant as the first impact force. However, there is a noticeable change between the first two versions and the third one. The difference in amplitude of the second impact wave between the 0 degree and 30 degree IRJ that can be seen in the first two graphs is no longer present in the third version, where the amplitude of the second impact wave is the same for both IRJ models.

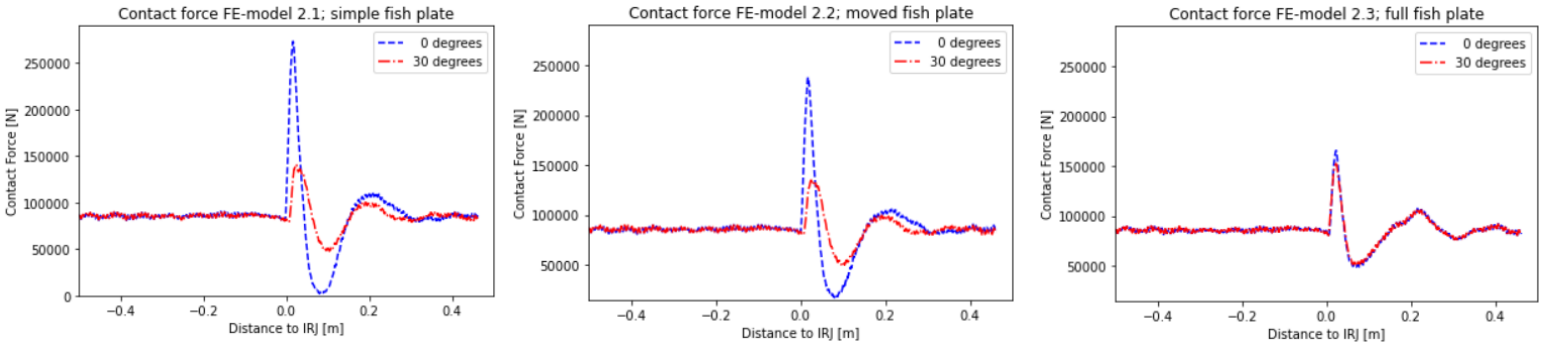

Figure 6.4: Contact force of different FE-model 2 versions; 0- and 30-degree IRJ

The impact ratio of the first impact peak force is shown in figure 6.4. The figure shows that the 0-degree IRJ has higher impact ratios, but also a significant reduction between the three versions. The impact ratio of the 30-degree IRJ, however, does not differ that much over the three versions and even results in a slightly higher impact ratio in the third version. The impact ratios of the square IRJ are very high in the first version, but comparable to (Cai et al., 2007) where an IRJ with rail height difference was studied. The third version results in impact ratios that are more expected with newer IRJs. In every version the angled IRJ does perform better with a lower impact ratio than the standard square IRJ.

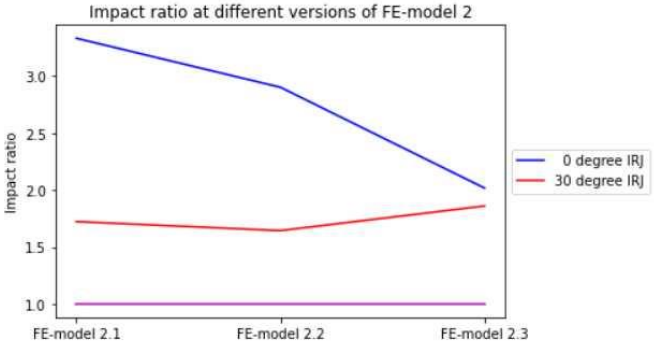

Figure 6.5: Impact ratios of the three versions of FE-model 2

6.1.2 Preliminary discussion of FE-model 2

Results show that the damping elements in FE-model 2 work and predict a more reasonable contact force. The damping elements ensure that the oscillations induced by the impact fade out and do not continue as in FE-model 1. The damping value is in range of other literature (Chapter 2).
An interesting observation is the fact that there is no drop in contact force before the IRJ impact occurs. This is most likely caused due to the way the contact force graph is combined out of two graphs, one for each rail. When a rail height difference is present there will still be contact with rail 1 at the moment the wheel impacts the edge of rail 2. If the 'step up' is high enough then the wheel will fully impact rail 2 before losing contact with rail 1, which will result in the disappearance of the drop in contact force.

The resulting impact force of all three FE-model 2 versions shows the biggest difference in the case of the square. The difference in these versions is the fishplate location and cross section. In mechanical terms the difference between the versions is the angular stiffness of the joint and how well deflection of the two rail ends is coupled. FE-model 2.1 has a really low bending stiffness and quite some slip between the plates and the rails, leading to a dipped joint with rail height difference. In FE-model 2.3 the bigger fish plates increase the bending stiffness and this version has less slip because the fish plates are higher and have less place for movement. Figure 6.6 illustrates this by showing the vertical displacement of the rail ends for FE-model 2.1 and 2.3. This height difference is expected to cause the difference in impact ratios, because the wheel will hit the rail end before rolling over it.
In case of the angled IRJ there was not a lot of difference in impact ratio. It was lower than the square IRJ in all three model versions. Due to the angle the relative rail height difference between the two rail ends can be overcome more smoothly. Therefore, the various versions of fish plates have less effect. In the case of FE-model 2.3, which simulates a stiffer joint with less 'step up', the angled IRJ performs worse with a higher impact ratio than the simulation of FE-model 2.1. In all three model versions the nominal gap remained at 8mm, so with a stiffer joint the increase in longitudinal gap gets more important than the 'step up'.

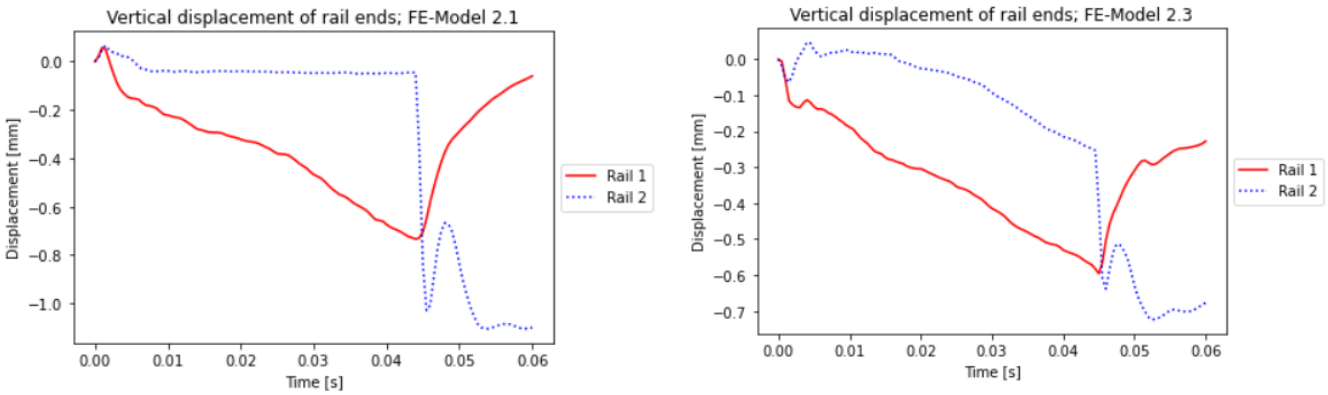

Figure 6.6: Displacement of rail end 1 and rail end 2; (left) FE-Model 2.1 with clear drop of rail 2 only at impact; (right) FE_Model 2.3 with rail 2 displacing with rail 1

6.1.3 Results from FE-model 2 with all angled IRJs

The previous simulations were performed with only two IRJ models: 0 degree and 30 degrees. These simulations showed that the angled IRJ performed better, likely due to the rail height difference. FE-model 2.3 resulted in impact ratios of both IRJ models which were closest to impact ratios from other literature (Chapter 2). Using FE-model 2.3 two more angles were simulated. It is expected that with a larger angle the impact force will be lower due to a more gradual transition from rail to rail.

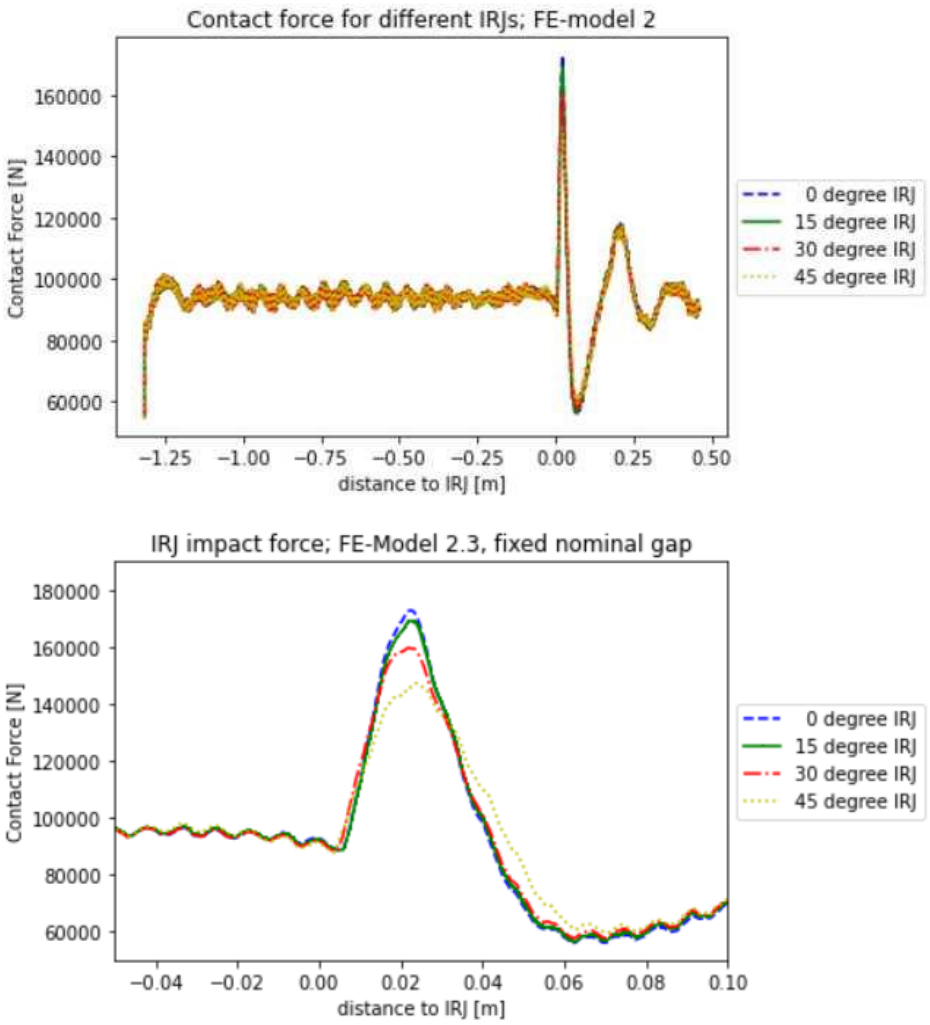

Figure 6.7: Contact force of FE-Model 2.3; 0, 15, 30 and 45 degree joint with fixed nominal gap

Figure 6.7 shows the contact force in the case of the four modelled IRJs. Before the IRJ these four types show the same steady contact force. At the peak impact force a difference is observed. The larger angled IRJ results in a lower peak impact force. The benefit of a 15 degree IRJ is quite small, whereas the benefit of a 45 degree IRJ is significant. After the peak impact force all four IRJ types quickly converge to the same contact force. The second impact peak is equal for all four IRJ types.

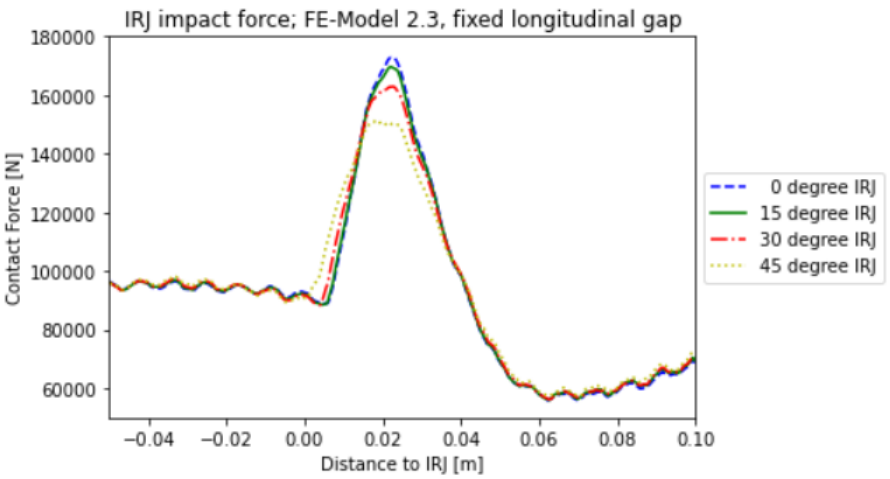

Figure 6.8: Contact force of FE-Model 2.3; 0, 15, 30 and 45 degree joint with fixed longitudinal gap

The same simulations were also performed with a fixed longitudinal gap of 8mm, there is no larger gap due to a larger angle. The results are presented in figure 6.8. The contact forces are similar to the previous simulations, with the IRJ of 45 degrees resulting in the lowest peak force. The dip after the first peak force is not observed for all IRJ types. The second impact wave and the contact force before the IRJ are equal for all IRJ types simulated.

6.2 Discussion of results from FE-Model 2

FE-model 2 showed that an angled IRJ results in lower impact forces compared to the square IRJ. His is caused by the height difference between the two rail ends mentioned before. This height difference causes a very high peak force because the wheel hits this 'step up' frontally. At an angled IRJ this 'step up' can be overcome more gradually. A larger angle is assumed to cause a more gradual transition. This is backed up by the graphs and figures in this chapter. In contrast to FE-model 1 the angled IRJ performs better when the nominal gap is fixed at 8mm ánd when the longitudinal gap is fixed at 8mm. It indicates that with a 'step up' present, the increase in gap length is less significant. The impact ratios for the FE-model 2 simulations are quite high for a new profile IRJ. When considering the height difference however, the ratios are more reasonable. (Cai & Wen, 2007) showed similar results for an analysis of IRJs with a height difference. Modelling a 'loose bolt' IRJ was not the initial aim of the second model in this thesis, but it does provide some interesting insight. Modelling a rail height difference may not have taken place otherwise.

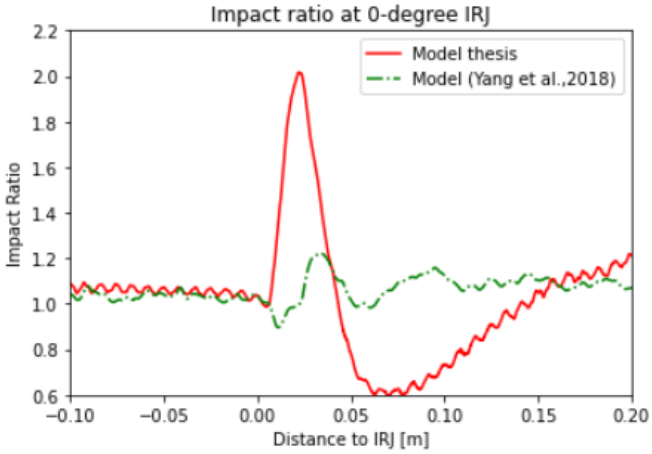

Figure 6.9: Impact ratio comparison of FE-Model 2.3 and (Yang et al., 2018)

6.2.1 Results with higher support stiffness

In figure 6.9 can be seen how much higher the impact ratio of this thesis' FE-model 2 is compared to (Yang et al., 2018). The aim was to create a more similar performing model. Due to the simplifications made a perfect fit was never expected, but the results of FE-model 2 were more in line with a loose joint scenario. In an attempt get the FE-Model 2 more in line with (Yang et al., 2018), the support stiffness was increased. The first time the new stiffness value for the spring elements became 10 times the calculated equivalent stiffness. In a second iteration a value of 20 times the equivalent stiffness was used. The slight variation in spring stiffness between the concrete and wooden sleepers remains.

Simulations were performed with the models with increased support stiffness values for all angled IRJs. The impact ratios resulting from these simulations are presented in figure 6.10. In the same figure are the impact ratios that resulted from FE-model 2 with equivalent support stiffness values. All simulations results are with the fixed nominal gap. It was presented that the extra gap width, due to a fixed nominal gap, causes significantly higher impact ratios. If the simulations considering the higher support stiffness values predict that the angled IRJ performs better than the square IRJ it is assumed this is also true at a fixed longitudinal gap.

A few things can be observed from figure 6.10. With the higher support stiffness value, the impact ratio for each angle is lower. However, the square IRJ benefits more and the 45-degree IRJ the least. In other words, by increasing the support stiffness value the angled IRJ becomes less effective with less difference in impact ratio between the angled and square IRJs.

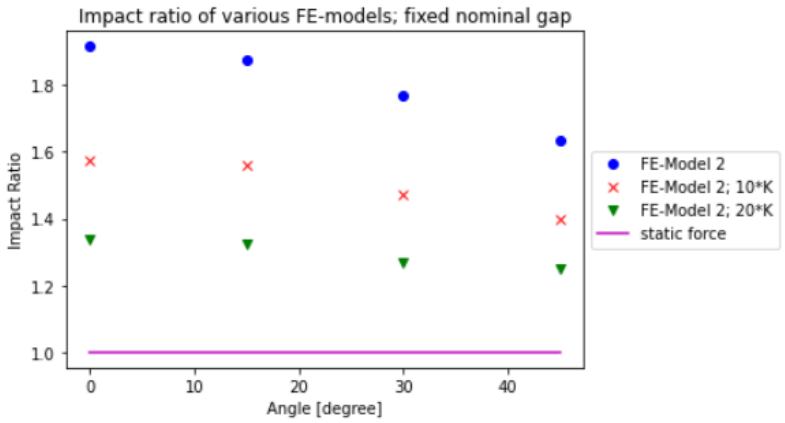

Figure 6.10: Impact ratio FE-Model 2 per simulated angled Joint

6.2.2 Discussion of 10/20K results

The fact that the impact ratios decrease when the support stiffness is increased is that this higher support stiffness causes less rail displacement. The rail ends are more 'fixed' in position because with a higher stiffness more force is required to get the same amount of displacement. This causes the rail height difference to be less. When the difference in rail height between rail 1 and rail 2 was investigated during the simulations, the results showed that just before impact the height difference was 0.1mm in the model version using a 20 times higher stiffness value. When the height difference is reduced the angled IRJs show less reduction of impact ratio. The graphs in figure 6.10 become more horizontal, indicating the mentioned lesser change in impact ratio.

It should be mentioned that the damping value remained the same and the stiffness value was only changed in the explicit simulation for efficiency reasons. Due to the change the wheel 'bounces' more starting from the same implicit solution. This meant that the simulation results became inaccurate at higher stiffness values, with the 20 times stiffness value simulation already an edge case.

In figure 6.11 the impact ratio of the two simulations with a higher support stiffness value are presented. These are compared to the ratio resulting from (Yang et al., 2018). The graphs become more similar with an increased stiffness. The model simulating a 20 times greater support stiffness value quite closely resembles (Yang et al., 2018) and better matches the aim of this model. However, it should be noted that the models reported in this thesis uses a larger gap width of 8mm, instead of the 6mm used in (Yang et al., 2018). Due to the larger gap a higher impact ratio is expected for the model reported in this thesis. In terms of impact ratio FE-model 2.3 with a 10 times higher support stiffness value is considered to best resemble (Yang et al., 2018).

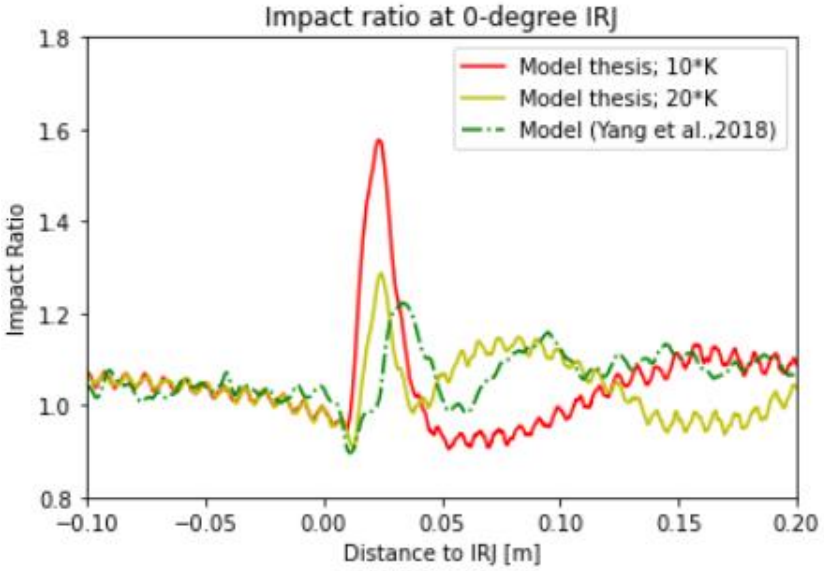

Figure 6.11: Impact ratio comparison of the high stiffness versions FE-Model 2 and (Yang et al., 2018)

6.3 Conclusions from FE-model 2

FE-model 2 performed differently than expected in the first simulation. The rail height difference explained why the results were different. These results did provide some interesting insights into angled IRJs. The model proved reliable keeping the rail height difference in mind. It showed that with a degraded or 'loose' IRJ the angled versions perform better, resulting in lower peak impact forces. This showed to be the case for simulations with a fixed nominal gap or a fixed longitudinal gap.
New versions of FE-model 2 were created with an increased support stiffness value. These changes caused less rail height difference and therefore lower impact forces. The lower rail height difference meant that the angled IRJs had less effect on the Impact ratio. The IRJs were modelled with a fixed nominal gap. FE-Model 1, which simulates infinite support stiffness, showed that the gap change was a significant reason for impact ratio change. Together with the FE-Model 2 results these indicate that there is a situation where the disadvantage of the gap change is negated by the benefit of the angled IRJ at rail height differences.

7 FE-Model 3: ‘Factory New’

A final adjustment to the FE-model covers the slip between the fishplates and the rail. Due to this slip the two rails may have displace vertically relative to each other, creating a ‘step up’ and a considerably larger impact force. Although this slip does occur in the field, it is not something assumed to happen to every IRJ. New IRJs are assumed to cause little to no difference in relative vertical rail displacement. Therefore, a change was made in the FE-model to better simulate the ‘Factory New’ conditions IRJs.
In this FE-Model 3 the coupling of nodes is used to define a more equal displacement of both rail ends. From each side of the rail web a few nodes were selected to couple to corresponding nodes from the side of both fish plates. This way there is no slip between the rail and fish plates, and the only difference in rail height is caused by the deformation of the rail itself and the deformation of the fish plates.

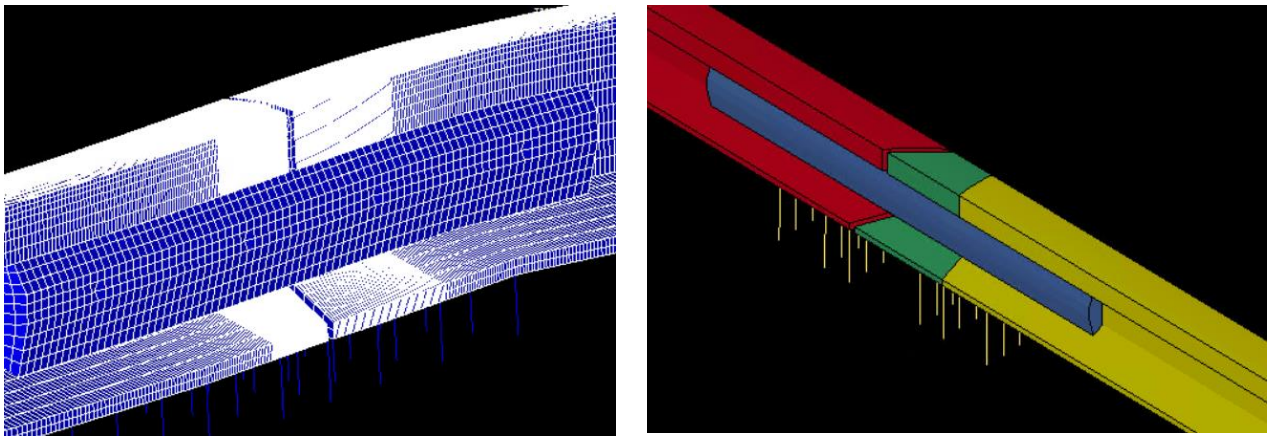

Figure 7.1: FE-Model 3; (Left) meshed IRJ with minimum rail height difference; (Right) angled IRJ of 30-degrees

7.1 Results from simulations

As with the previous FE-models, 4 simulations were performed with the IRJ angle ranging from 0 (square IRJ) to 45 degrees. For these simulations the nominal gap was fixed at 8mm, so a larger angle means a longer longitudinal gap. From figure 7.2 can be seen that the simulation result looks very similar to the previous models, indicating that the changes do not cause the model to deviate from expected results. The contact force stabilizes quickly and oscillates around the static load value until the impact at the IRJ. A clear drop in contact force can be observed there, after which impact occurs. At this point some differences due to the different IRJ angles can be spotted. At the second impact wave there is no difference anymore. The part before the impact with the IRJ is also similar for all four simulations.

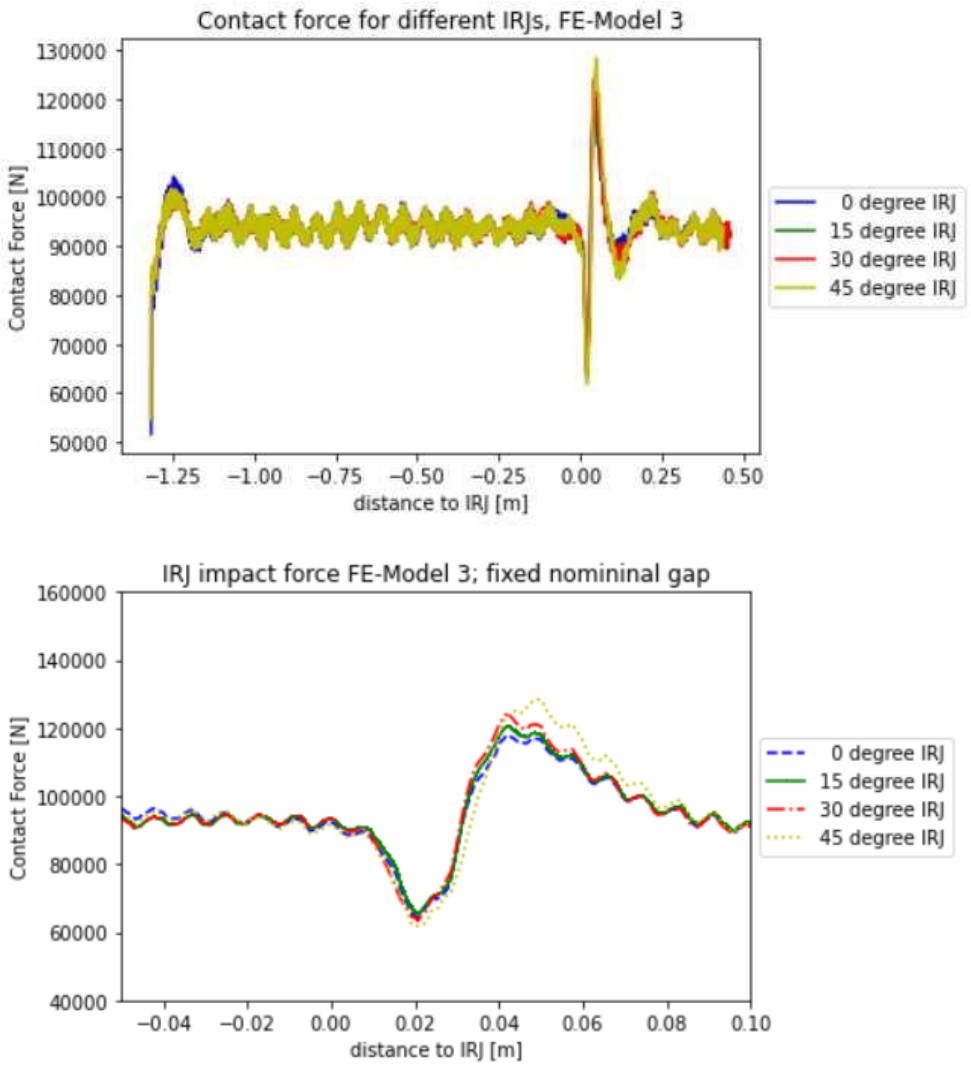

Figure 7.2: Contact force of FE-Model 3; 0, 15, 30 and 45 degree joint with fixed nominal gap

Figure 7.2 also presents the same graphs, zoomed in on the part where the IRJ impact occurs. The 45-degree angled IRJ creates the highest impact force, and the standard square IRJ the lowest. This result is comparable to FE-model 1.

The simulations discussed using FE-model 3 were performed again, but this time the longitudinal gap is fixed at 8mm. Figure 7.3 presents the contact force results of these simulations. The contact force stabilised quickly and the dip in contact force before the impact is clearly visible again. However, this time there is no significant change in contact force between the different angled IRJ variants.

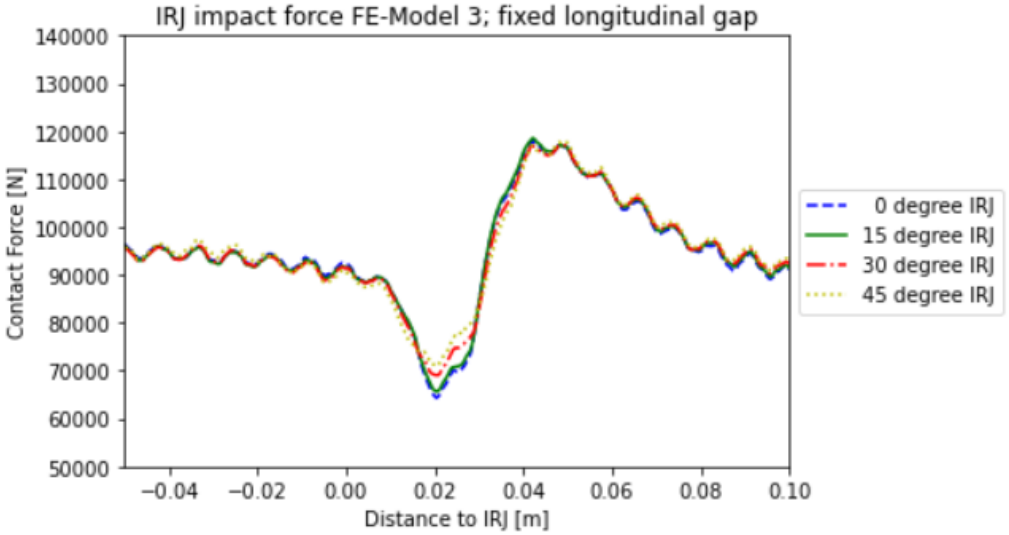

Figure 7.3:Contact force of FE-Model 3; 0, 15, 30 and 45 degree joint with fixed longitudinal gap

Although it almost appears that there is no difference between the four graphs in figure 7.3, they are in fact different graphs of different simulations. At the dip in the contact force the four different graphs are visible, where the smaller square and 15 degree IRJ show a larger drop in contact force than the other angled IRJs.
From the previous figures, the impact ratios are calculated for the first impact peak force. These are presented in figure 7.4. From these graphs can be observed that that when the gap width size increases the impact ratio increases as well. When the gap width is fixed in longitudinal direction there is no significant change in impact ratio noticeable.

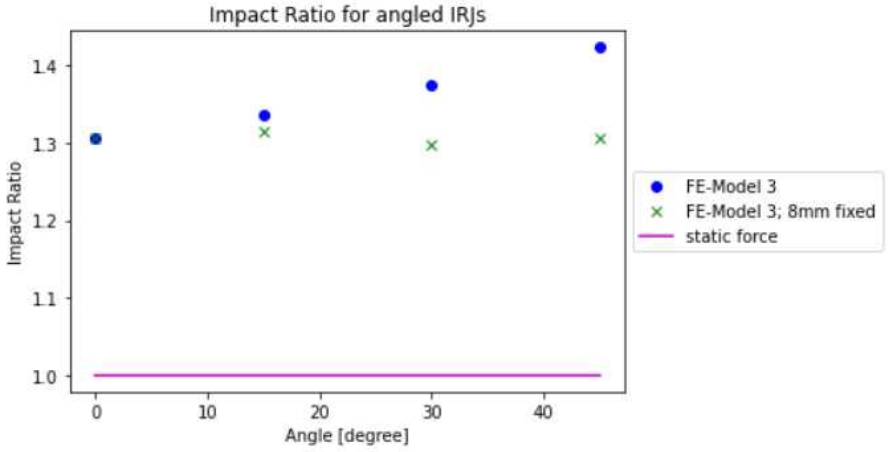

Figure 7.4: Impact ratio per angled IRJ, FE-Model 3

7.2 Discussion of results

The results from FE-model 3 show a similar story as the results of FE-model 1. With a fixed nominal gap, the longitudinal gap increases at angled IRJs. This larger gap causes a higher impact force. If the longitudinal gap is fixed the angled IRJ does not cause any significant difference in impact force or ratio.

In figure 7.5 the impact ratio of a square IRJ is plotted during the impact. A comparison is made between FE-model 3 reported in this thesis and a square IRJ simulation from (Yang et al.,2018). Although both the models show some differences, the general shape is similar. It should be noted that the simulation from (Yang et al., 2018) uses a 6mm gap. Therefore, a lower impact ratio is to be expected for that simulation. The similar shape combined with an impact ratio below 1.4 shows this thesis' FE-model 3 can simulate the behaviour of a new condition IRJ with accurate and suitable results. It also shows that in this case the angled IRJ does result in lower impact ratios. On the contrary, with a fixed nominal gap an angled IRJ causes a larger impact force than the square IRJ.

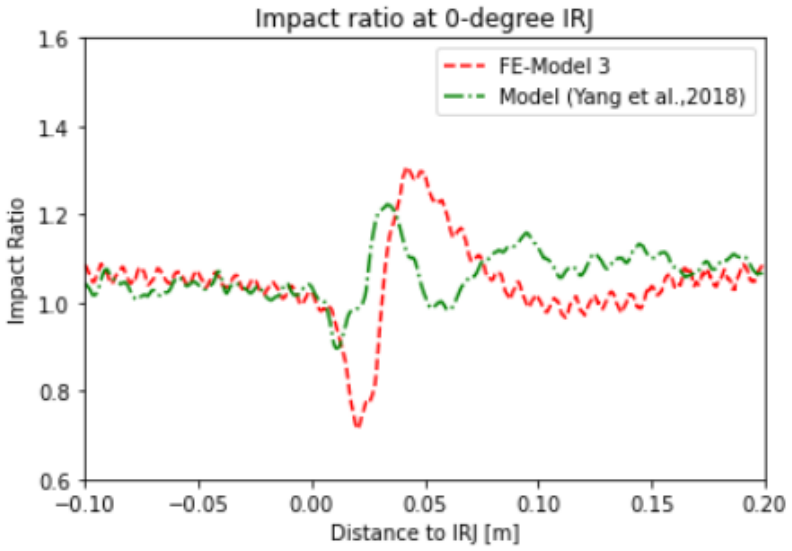

Figure 7.5: impact ratio comparison FE-Model 3 and (Yang et al.,2018)

8 Discussion of Total Simulation Results

This thesis has reported results of different simulations. Three main version of the FE-model were created and used to see if an angled IRJ would result in lower impact forces. In this chapter a final comparison of the different simulation results of the three FE-models are presented.

8.1 Fixed Nominal Gap

The first simulations performed by the three FE-models were on IRJs with a fixed nominal gap. Per FE-model the results were different and an angled IRJ did not perform better in every model. Figure 8.1 shows that only FE-model 2 resulted in a lower impact ratio for angled IRJs compared to standard square IRJs.

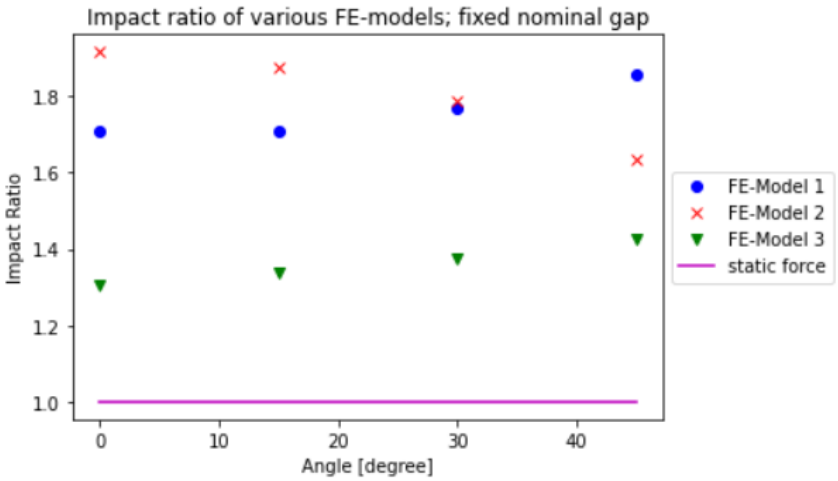

Figure 8.1: Impact ratio of the FE-Models, per angled IRJ; fixed nominal gap

FE-model 1 and 3 both show that an angled IRJ results in higher impact ratios. The main reason for this behaviour is the gap increase due to the angle explained in (Chapter 3). FE-model 2 simulated a degraded IRJ, which enabled rail height differences to occur. In this situation the angled IRJ showed significant lower impact forces on larger angles. It is suggested that at the square IRJ a wheel would collide with the rail end, thereby pushing it down and rolling further. The angled IRJ will enable a smoother transition of the rail height difference.

8.2 Fixed Longitudinal Gap

The simulations with the square and angled IRJs were also performed on all three FE-models with a fixed longitudinal gap where an angle increase has no effect on the gap width. All other parameters are equal to the simulations in the previous section.
Figure 8.2 shows the results of the simulations. In contrast to the previous section these simulation results show no FE-model predict that angled IRJs would result in higher impact forces. FE-model 1 and FE-model 3 show a similar impact ratio for all simulated IRJs, both the standard and angled version. This strengthens the fact that the gap increase plays a major part in the impact forces.

FE-model 2 shows with these simulations that the angled IRJ performs better than the standard IRJ, just as with the fixed nominal gap. This model simulated a rail height difference, meaning that the gap width difference appears to have less effect than the rail height difference.

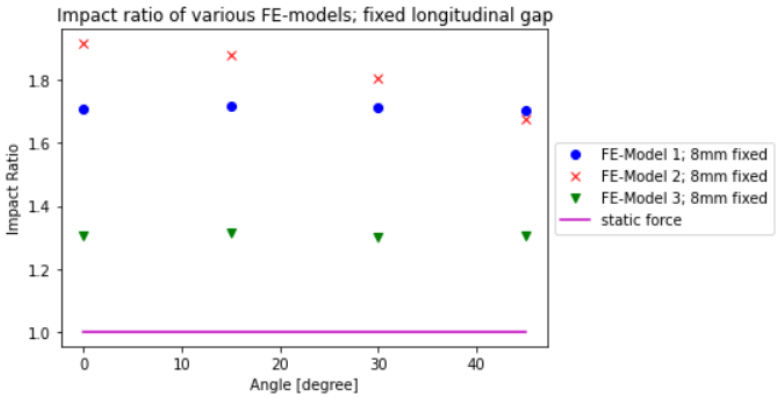

Figure 8.2: Impact ratio of the FE-Models, per angled IRJ; fixed longitudinal gap

8.3 Stiffness change

In FE-model 2 the rail height difference resulted in high impact forces and thus high impact ratios. This was not expected from the start and an attempt was made to reduce the rail height difference. The support stiffness was increased tenfold on a model with a fixed nominal gap. An increased stiffness means less displacement if the acting force remains equal, thus reducing the rail height difference. This had a clear effect and the impact ratio lowered for both IRJ types. Not only that, the benefit of the angled IRJ became less.

A final version was simulated with a support stiffness value of 20 time more than the calculated equivalent value based on (Yang et al., 2018). This again resulted in lower impact ratios. It also meant that there was again less difference between the angled and standard IRJs. This effect indicates that there is a rail height difference value where the disadvantage of a larger gap for an angled IRJ is equal to the benefit of a smooth rail height transition.

The value for the damping elements has remained the same when the stiffness values changed. The damping has become less effective with the stiffer spring elements. At the limit the stiffness would be infinite and this is the case in FE-model 1. A version with a stiffness value of 30 times the equivalent value already resulted in more oscillations and a non-accurate contact force.

9 Sensitivity Research

Since FE-model 2 showed the most promising results for angled IRJs a sensitivity analysis was performed using this model. The effects of certain parameter changes on the model results were analysed. The parameters varied for the sensitivity analysis are the applied wheel load and the velocity. These parameters may vary a lot from place to place and may provide some insight into the question whether or not an angled joint would perform better in certain conditions.

9.1 Wheel Load

A wide variety of trains are used across the world, and the different trains may all have a different wheel load. A light 'Sprinter', a small commuter train from the Dutch Railways, has a wheel load of almost 90kN (Nederlandse Spoorwegen, n.d.). Compared to that, the locomotives of the high speed trains used in the Netherlands have a weight of 87 tonnes on 4 axles (Akiem, 2017), resulting in a wheel load of almost 110kN. These numbers are comparable other European railways. Looking outside Europe there are more significant differences. In Australia the heaviest freight train reached an axle load of 40tonnes (Kirk, 2018), resulting in a wheel load of nearly 200kN. These different wheel loads could result in different outcomes of whether or not an angled IRJ is beneficial. The wheel load was altered for all four IRJ designs, and simulations were performed at 70, 90, 110, 130 and 150kN. The resulting contact forces at the point of impact of these simulations are shown in figure 9.1.

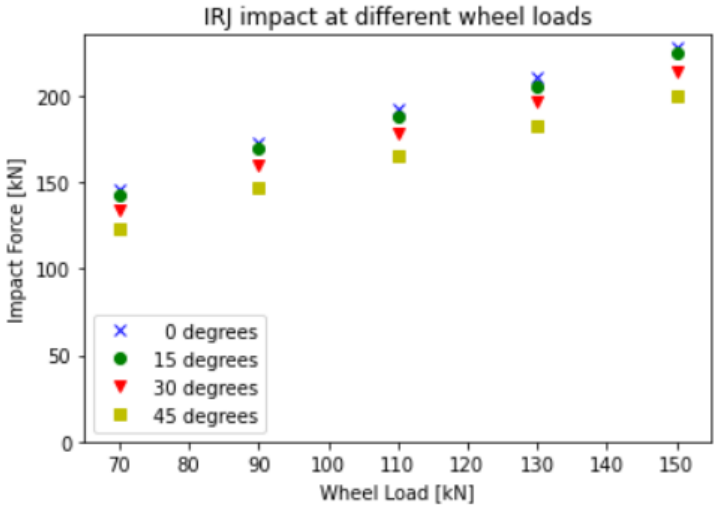

Figure 9.1: Contact force per wheel load; 0-, 15-, 30- and 45-degree IRJ

With an increase in wheel load the total impact force at the IRJ also increases, which is as expected. The more interesting result is the way the impact force increases versus the wheel load increase. This impact ratio is shown in figure 9.2.

The impact ratio decreases as the wheel load increases, which means that the relative increase in dynamic force on the IRJ is less with a higher wheel load. It also appears that the decrease of impact ratio per velocity change gets less at higher wheel loads and that there is a limit. Otherwise a high enough wheel load would result in no impact at all, which is not realistic.
The graph looks very similar for both the standard IRJ and the angled ones. However, the angled IRJ shows a lower impact force at all wheel loads, with the difference compared to the normal IRJ decreasing slightly at higher wheel loads. It can be concluded that the angled IRJ performs better and that there is no real optimum regarding the wheel load.

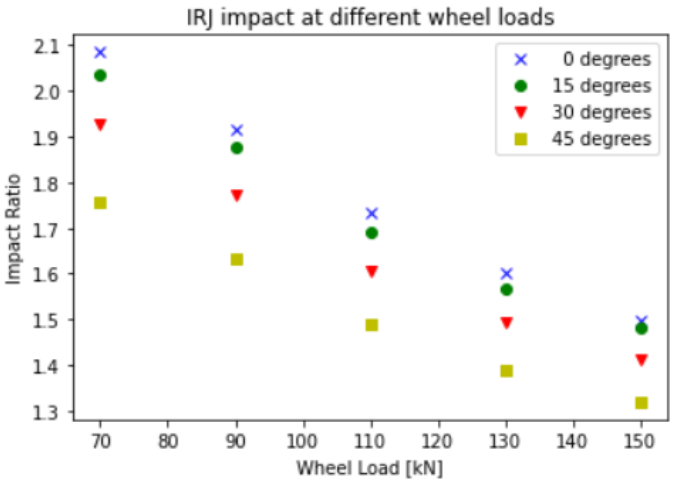

Figure 9.2: Impact ratio per wheel load; 0-, 15-, 30- and 45-degree IRJ

The results of the varying wheel load correspond with (Mayers, 2018), which found a non-linear relation when measuring strains of a square IRJ at different wheel loads.

9.2 Velocity Change

The velocity with which a train passes an IRJ is highly variable and depends for instance on location (near a station or open track), the type of train (high speed train or slow cargo train) and the maximum velocity allowed on the track. The different velocities may have various effects on how the IRJ will perform. (Cai et al., 2007) did a similar study into velocity change involving only the square cut IRJ. In this research it was found that the velocity linearly affected the impact force, and that a higher velocity results in a higher impact force. Their conclusion can be seen in figure 9.3.

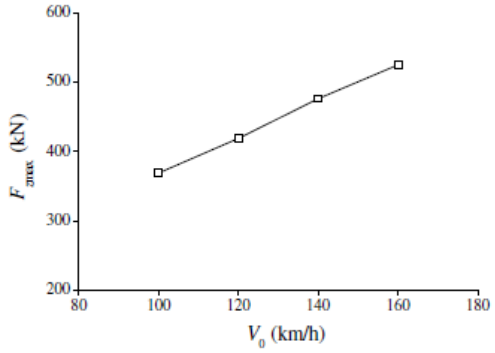

Figure 9.3: Results of contact force increase per velocity of (Cai et al., 2007)

For this thesis the same kind of sensitivity analysis was performed. This thesis so far showed that an angled IRJ may result in lower impact forces. It may be the case that at other velocities the outcome is different. The factors analysed are the reduction of impact force per velocity, and the reduction per different IRJ. The simulations are performed with all four types of angled IRJ. The velocity was varied between 80km/h and 140km/h. This range contains the most common maximum velocities of the tracks in the Netherlands (Prorail,2020).

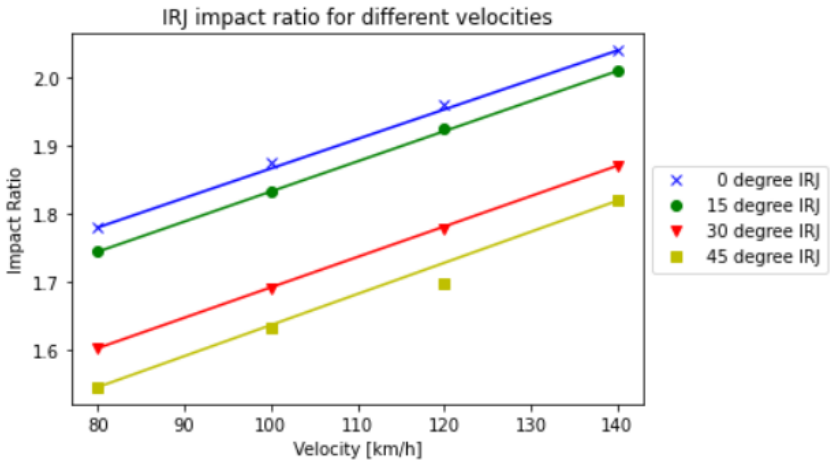

Figure 9.4: Impact ratio per velocity; 0-, 15-, 30- and 45-degree IRJ

Figure 9.4 shows the results for the simulations performed at different velocities. It shows the impact ratio of the angled IRJs per velocity. Just as (Cai et al., 2007) had found, the results show a linear relationship where a higher velocity results in higher impact forces. This observation also holds for the angled IRJs. Another interesting relationship is the reduction in impact ratio over different velocities. Figure 8.4 shows parallel graphs, which show that the benefit of angled IRJs resulting in lower impact ratios remains roughly the same. This means that in terms of velocity there is no optimal situation to use any specific angled IRJ, other than that in general a lower velocity results in a lower impact ratio and a larger angle results in lower impact forces.
The 120km/h simulation is a bit off from the rest. The reduction in impact ratio is slightly more for the 45 degree IRJ. The impact ratio is lower than expected with an assumed linear relationship. There is no clear indication why this is the case, it seems an outlier. With heavy dynamic problems such as impact simulations some numerical variation is not uncommon. In this case the difference between the value of the outlier and the expected value is about 2%, which is considered to be well within margin and does not justify rejecting the simulation results.

10 Concluding remarks

In this thesis a study is presented that was performed on angled Insulated Rail Joints (IRJs). The effect of angled IRJs on the peak wheel-rail impact force was investigated. A literature study showed that although the angled IRJ is in use it is also already abandoned in some places. Despite the experiences on the subject the existing research is marginal.
To simulate the wheel-rail interaction a sequential implicit-explicit FE method was used. A series of models were built in ANSYS/LS-DYNA, based on algorithms and solution procedures presented in (Yang et al., 2018). Simplifications such as a coarser mesh, direct forces instead of sprung masses and combined spring/damper elements were used to reduce the simulation times and enable faster adjustments. A comparison with a well validated model from (Yang et al.,2018) and Hertzian contact theory showed the new model was reliable and efficient for the purpose of this thesis.

Three FE-models were made with an IRJ of 0, 15, 30 and 45 degrees. FE-Model 1 was the most basic version using a fully constrained rail foot simulating infinite support stiffness. The model showed that with a fixed nominal gap the angled IRJ had a higher impact force. If the longitudinal gap was fixed the model showed no difference in impact force.
FE-model 2 used spring and damper elements to model the track substructure, with parameters derived from (Yang et al.,2018). This model showed that the angled IRJs had lower impact forces and that the amplitude of the impact forces decreased with an increase of the angle. This was the case for both the version with fixed nominal gap and the version with fixed longitudinal gap. A height difference between the two rail ends occurred when the wheel passed the joint. The simulations indicate that the wheel can pass more smoothly over an angled joint. To reduce the height difference the stiffness of the support springs was increased by 10 and by 20 times. These versions showed that the angled IRJ gave less benefit with the smaller height difference. This indicates that the advantage of the angled IRJ can depend on the support stiffness and leads to the expectation of a limit where the advantage of the angled IRJ is equal to the disadvantage of the increased longitudinal gap.
Finally, FE-model 3 used node coupling to define no slip between fish plate and rail web, representing a new tight bolted joint. This minimum rail height difference gave similar results as FE-model 1. With a fixed longitudinal gap there is no clear benefit from using angled IRJs, whereas with a fixed nominal gap the angled IRJ performed worse as the longitudinal gap increases per angle.

Because FE-model 2, which represented a degraded support condition joint, showed that the angled IRJ was beneficial, this model was used to vary the velocity and the wheel load and study the sensitivity of the wheel-rail impact force on it. This resulted in a linear relationship of impact ratio and the velocity and a non-linear relationship with the applied wheel load. The benefit of the angled IRJ does not change with the velocity, whereas the wheel load changes the amount of impact reduction slightly.

10.1 Recommendations

The results and conclusions of this thesis give rise to some advice. It should be noted that there are more factors which may influence the choice between angled or square IRJs than only the ones discussed in this thesis.

The results indicate that the angled IRJ is most beneficial with an in-service or degraded IRJ with rail height differences, whereas depending on the end post thickness requirements at a new IRJ there is no advantage or even a disadvantage using angled IRJs. It therefore depends on the use, service life and maintenance regime of the tracks if an angled IRJ would be recommended. In western Europe the joints are often maintained to keep them in new condition, and in these situations the square IRJ is advised.
For tracks with less rigorous maintenance schemes such as heavy haul tracks or in remote areas, the angled IRJs may be advised based on this thesis, as they perform better if there are already some degraded support conditions. The lower impact force can then keep the IRJ from deteriorating faster.

The reason why angled joints are no longer used in certain places is expected to be due to high stresses in the tip of the joint. This is an interesting point for further research, which should be possible with a slight change of the presented FE-models in this thesis.
With the angled IRJ reducing the impact forces it can be of interest to study the frequencies and vibrations caused by it. Although for 0-degree IRJs this is studied already it could be different for angled IRJs as these showed to generate less noise (Ataei et al., 2016).
In this thesis only a new rail profile is used. With that new profile the in-service ‘loose IRJ’ model showed that the angled IRJ is beneficial. An interesting study is to do the research done in this thesis but with worn profile rails, and to check if the worn profile provides the same results.
The lateral displacement was not considered but could have more influence on angled IRJs than square IRJs due to the eccentricity. This is not yet studied and would be possible with the presented FE-models in this thesis.

11 References

Akhtar, M., Davis, D., & O'Connor, T. (2007). *REVENUE SERVICE EVALUATION OF ADVANCED DESIGN INSULATED JOINTS*. Retrieved from https://TransportationTechnologyCenter.com

Akiem. (2017). *BR186 Traxx*. Retrieved from https://www.akiem.com/wp-content/uploads/2018/07/BR-186-EN-1.pdf

ANSYS inc. (2011). *ANSYS Mechanical APDL Element Reference*. Retrieved from https://www.mm.bme.hu/~gyebro/files/vem/ansys_14_element_reference.pdf

Askarinejad, H., & Dhanasekar, M. (2016). A Multi-Body Dynamic Model for Analysis of Localized Track Responses in Vicinity of Rail Discontinuities. *International Journal of Structural Stability and Dynamics*, *16*(09), 1550058. https://doi.org/10.1142/s0219455415500583

Askarinejad, H., Dhanasekar, M., & Cole, C. (2012). Assessing the effects of track input on the response of insulated rail joints using field experiments. *Proceedings of the Institution of Mechanical Engineers, Part F: Journal of Rail and Rapid Transit*, *227*(2), 176–187. https://doi.org/10.1177/0954409712458496

Ataei, S., Mohammadzadeh, S., & Miri, A. (2016). Dynamic Forces at Square and Inclined Rail Joints: Field Experiments. *Journal of Transportation Engineering*, *142*(9), unknown. https://doi.org/10.1061/(asce)te.1943-5436.0000866

Australian Rail Track Corporation. (2006, November). *Manufacture and testing of pre- assembled glued insulated rail joints*. Retrieved from https://extranet.artc.com.au/docs/eng/track-civil/procedures/rail/eta-01-01.pdf

Bundesamt für Umwelt BAFU (Swiss), Weidmann, U., Hecht, M., & Maibach, M. (2015). *Stand der Forschung und Forschungsbedarf im Be-reich Eisenbahnlärm*. Retrieved from https://www.bafu.admin.ch/bafu/de/home/themen/laerm/fachinformationen/massnahmen-gegen-laerm/massnahmen-gegen-eisenbahnlaerm/ressortforschung-eisenbahnlaerm.html

Cai, W., Wen, Z., Jin, X., & Zhai, W. (2007). Dynamic stress analysis of rail joint with height difference defect using finite element method. *Engineering Failure Analysis*, *14*(8), 1488–1499. https://doi.org/10.1016/j.engfailanal.2007.01.007

Charlton, Z. (2007). *Innovative Design Concepts for Insulated Joints*. Retrieved from https://www.semanticscholar.org/paper/Innovative-Design-Concepts-for-Insulated-Joints-Charlton/e46c875cb0eca4fe8db237e9f647b0d70d851dd1

Dalton, P. J. (1908). *877057*. New York, US: US Patent Office.

Dangre, H. (2019). *A Review On Insulated Rail Joints (IRJ) Failure Analysis.* Retrieved from http://www.ijarp.org/published-research-papers/jan2019/A-Review-On-Insulated-Rail-Joints-irj-Failure-Analysis.pdf

DB Training & Bahn. (2016). DB Training & Bahn Fachverlag 2016. Retrieved 2020, from https://www.bahn-fachverlag.de/en/blog/verlag/partner/db-training-learning-und-consulting/dbt_logo_2016_grau_cmyk-2/?

Dhanasekar, M. (2013). Manual for the Design, Installation and Maintenance of Insulated Rail Joints. *CRC for Rail Innovation*, 2–87. https://doi.org/10.13140/RG.2.1.3770.0569

Dhanasekar, M., & Bayissa, W. (2011). Performance of square and inclined insulated rail joints based on field strain measurements. *Proceedings of the Institution of Mechanical Engineers, Part F: Journal of Rail and Rapid Transit*, *226*(2), 140–154. https://doi.org/10.1177/0954409711415898

Eisenbahn-Bundesamt. (2009, September). EBA - Zulassung für den Isolierstoß der Bauart IVB 30˚. Retrieved January 2020, from https://www.eba.bund.de/SharedDocs/Standardartikel/DE/Zulassungen/Oberbau/Sonstiges/21.61-21izbo-009-2101-009(503_09-Zul.html

Eisenbahn-Bundesamt. (2015, March). EBA - Sonstiges - Zustimmungen im Einzelfall - Verlängerung der Zulassung für Isolierstoß Bauart IVB 30 °. Retrieved January 2020, from https://www.eba.bund.de/SharedDocs/Standardartikel/DE/Zulassungen/Oberbau/Sonstiges/21.61-21izbo-020-2101-009(503_09-Verl).html?nn=1622668

El-sayed, H. M., Lotfy, M., El-din Zohny, H. N., & Riad, H. S. (2018). A three dimensional finite element analysis of insulated rail joints deterioration. *Engineering Failure Analysis*, *91*, 201–215. https://doi.org/10.1016/j.engfailanal.2018.04.042

Elshukri, F. A. (2016, January). *An Experimental Investigation and Improvement of Insulated Rail Joints (IRJs) End Post Performance.* University of Sheffield. Retrieved from https://www.researchgate.net/publication/280445054

Esveld, C. (2001). *Modern railway track* (2nd ed.). Zaltbommel, Nederland: MRT-productions.

European Commission. (2020, December). The journey begins – 2021 is the European Year of Rail! Retrieved 2021, from https://ec.europa.eu/commission/presscorner/detail/en/IP_20_2528

Gallou, M., Frost, M., El-Hamalawi, A., & Hardwick, C. (2018). Assessing the deflection behaviour of mechanical and insulated rail joints using finite element analysis. *Proceedings of the Institution of Mechanical Engineers, Part F: Journal of Rail and Rapid Transit*, *232*(9), 2290–2308. https://doi.org/10.1177/0954409718766925

Gallou, M., Temple, B., Hardwick, C., Frost, M., & El-Hamalawi, A. (2016). Potential for external reinforcement of insulated rail joints. *Proceedings of the Institution of Mechanical Engineers, Part F: Journal of Rail and Rapid Transit*, *232*(3), 697–708. https://doi.org/10.1177/0954409716684278

Hertz, H. (1882). Ueber die Berührung fester elastischer Körper. *Journal Für Die Reine Und Angewandte Mathematik (Crelles Journal)*, *1882*(92), 156–171. https://doi.org/10.1515/crll.1882.92.156

Himebaugh, A. K., Plaut, R. H., & Dillard, D. A. (2008). Finite element analysis of bonded insulated rail joints. *International Journal of Adhesion and Adhesives*, *28*(3), 142–150. https://doi.org/10.1016/j.ijadhadh.2007.09.003

Kirk, J. (2018). Fortescue opens the world's heaviest haul railway. Retrieved February 2021, from https://www.railwaygazette.com/news/fortescue-opens-the-worlds-heaviest-haul-railway/33125.article

Kroeze, E. (2019). NS Jaarcijfers 2019. Retrieved 2021, from https://nieuws.ns.nl/ns-jaarcijfers-2019--treinreiziger-gaat-er-in-5-jaar-fors-op-vooruit/

Mandal, N. K., & Dhanasekar, M. (2013, November). *STRESS ANALYSIS OF INSERTED RAIL JOINTS*. Conference: 10th World Congress on Railway Research. Retrieved from https://www.researchgate.net/publication/259240748

Mandal, N. K., Dhanasekar, M., & Sun, Y. Q. (2014). Impact forces at dipped rail joints. *Proceedings of the Institution of Mechanical Engineers, Part F: Journal of Rail and Rapid Transit*, *230*(1), 271–282. https://doi.org/10.1177/0954409714537816

Mandal, N. K., & Peach, B. (2010). An engineering analysis of insulated rail joints: A general perspective. *International Journal of Engineering Science and Technology*, *2010*(2), 3964–3988. Retrieved from https://www.researchgate.net/publication/50346113

Mayers, A. C. (2018, November). *An investigation of the structural mechanics of insulated rail joints*. https://doi.org/10.5204/thesis.eprints.122878

Movares. (2020, November 25). Voorgespannen ES-las. Retrieved 8 January 2021, from https://movares.nl/projecten/voorgespannen-es-las/

Nederlandse Spoorwegen. (n.d.). Materieel | Over NS | NS. Retrieved 2020, from https://www.ns.nl/over-ns/treinen-van-ns

Németh, A., & Fischer, S. (2018, March). *Field tests of glued insulated rail joints with polymer-composite and steel fishplates*. Retrieved from https://www.researchgate.net/publication/324056682_Field_tests_of_glued_insulated_rail_joints_with_polymer-composite_and_steel_fishplates

Németh, A., Major, Z., & Fischer, S. (2020). FEM Modelling Possibilities of Glued Insulated Rail Joints for CWR Tracks. *Acta Technica Jaurinensis*, *13*(1), 42–84. https://doi.org/10.14513/actatechjaur.v13.n1.535

ÖBB Infra. (2017). Publikationen. Retrieved 2020, from https://presse.oebb.at/de/publikationen

Papaioannou, I. (2018, October). *Experimental and numerical study on the optimisation of insulated rail joint dynamic behaviour*. Retrieved from https://repository.tudelft.nl

Plaut, R. H., Lohse-Busch, H., Eckstein, A., Lambrecht, S., & Dillard, D. A. (2007). Analysis of tapered, adhesively bonded, insulated rail joints. *Proceedings of the Institution of Mechanical Engineers, Part F: Journal of Rail and Rapid Transit*, *221*(2), 195–204. https://doi.org/10.1243/0954409jrrt107

Prakoso, P. B. (2012). The Basic Concepts of Modelling Railway Track Systems using Conventional and Finite Element Methods. *INFO TEKNIK*, *13*, 57–65. Retrieved from https://media.neliti.com/media/publications/66250-EN-the-basic-concepts-of-modelling-railway.pdf

ProRail. (2020, January). ProRail Jaarverslag 2019. Retrieved November 2020, from https://www.jaarverslagprorail.nl/verslag/kerncijfers

Quirchmair, M., Frobherg, E., & Loy, H. (2019, February). *Insulated rail joints: A solution to improve lifetime and performance at high maintenance track sections*. Retrieved from https://www.researchgate.net/publication/331379294

Quirchmair, M., Marschnig, S., & Fellinger, M. (2020). Isolierstöße im Gleis. *ZEVrail*, *144*(11/12), 420–429. Retrieved from https://www.researchgate.net/publication/348620455_REVIEWED_-_Isolierstosse_im_Gleis

Rail Infrabeheer. (2002). *Onderzoek naar bruikbare alternatieven voor ES- lassen in gelijmde uitvoering.* Utrecht, The Netherlands

Rijneveld, M. P. (2020, February). *Science Matchmaking: Onderzoek invloed van bladafval op detectieverlies*. Delft, Nederland: TUDelft.

Todhunter, I., & de Saint-Venant, A. J. C. B. (1889). *The Elastical Researches of Barré de Saint-Venant*. Amsterdam, Netherlands: Amsterdam University Press.

Van Beek, D. A. (1999). Hertzian elliptic contact. Retrieved 2020, from https://www.tribology-abc.com/calculators/e2_2.htm

Van Dyk, B. J., Edwards, J. R., Dersch, M. S., Ruppert, C. J., & Barkan, C. P. L. (2016). Evaluation of dynamic and impact wheel load factors and their application in design processes. *Proceedings of the Institution of Mechanical Engineers, Part F: Journal of Rail and Rapid Transit*, *231*(1), 33–43. https://doi.org/10.1177/0954409715619454

Voestalpine GmbH. (n.d.). Insulated Rail Joint IVB 30 / IVG 30 - voestalpine Turnout Technology Germany GmbH. Retrieved January 2020, from https://www.voestalpine.com/turnout-technology-germany/en/products/Insulated-Rail-Joint-IVB-30---IVG-30/

Vossloh AG. (n.d.). Glued insulated joints. Retrieved January 2020, from https://www.vossloh.com/en/products-and-solutions/product-finder/product_10562.php

Yang, Z. (2018). *Numerical Modelling of Wheel-rail Dynamic Interactions with an Explicit Finite Element Method*. Retrieved from https://repository.tudelft.nl/islandora/object/uuid%3A8acb9b48-bf77-45b2-a0d6-1cf6658f749e

Yang, Z., Boogaard, A., Chen, R., Dollevoet, R., & Li, Z. (2018b). Numerical and experimental study of wheel-rail impact vibration and noise generated at an insulated rail joint. *International Journal of Impact Engineering*, *113*, 29–39. https://doi.org/10.1016/j.ijimpeng.2017.11.008

Yang, Z., Boogaard, A., Wei, Z., Liu, J., Dollevoet, R., & Li, Z. (2018a). Numerical study of wheel-rail impact contact solutions at an insulated rail joint. *International Journal of Mechanical Sciences*, *138–139*, 310–322. https://doi.org/10.1016/j.ijmecsci.2018.02.025

Yang Z, Deng X, Li Z, Numerical modeling of dynamic frictional rolling contactwith an explicit finite element method, Tribology International (2018), doi: 10.1016/j.triboint.2018.08.028.

Zong, N., & Dhanasekar, M. (2013). Minimization of railhead edge stresses through shape optimization. *Engineering Optimization*, *45*(9), 1043–1060. https://doi.org/10.1080/0305215x.2012.717075

Zong, N., & Dhanasekar, M. (2015). Hybrid Genetic Algorithm for Elimination of Severe Stress Concentration in Railhead Ends. *Journal of Computing in Civil Engineering*, *29*(5), 04014075. https://doi.org/10.1061/(asce)cp.1943-5487.0000374

Zong, N., Wexler, D., & Dhanasekar, M. (2013, January). *Structural and Material Characterisation of Insulated Rail Joints*. Electronic Journal of Structural Engineering 13(1):75-87. Retrieved from https://www.researchgate.net/publication/288146670

Appendix A: Element Descriptions

The characteristics and properties of the elements used in this thesis are shown here. They can also be found in the manual of the software used (ANSYS inc., 2011). A short summary is given here.

SOLID185

SOLID-185 is an 8-node structural element used for 3D solid structures in implicit analysis. Each node has three degrees of freedom: translation in X-, Y- and Z-direction. The element enables simulating large deflections and strains, as well as plasticity, creep, hyper elasticity and stress stiffening. all mayor structural properties such as poisons ratio and Youngs modulus in three directions can be defined. Material properties are selected to be isotropic.
Although this element can be Prism- or tetrahedral-shaped, the best accuracy is achieved in hexahedral (brick) shape, which is used in this thesis. The software outputs the displacement of all nodes in three directions.

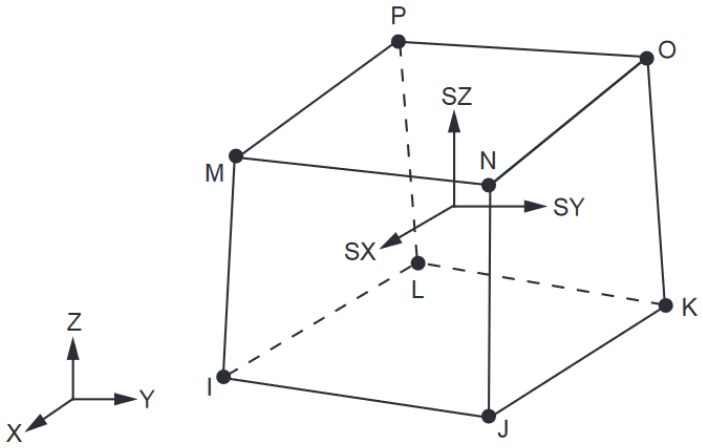

Figure A1: 8-node solid element

SOLID164

This element can be seen as the explicit variant of SOLID185, used for solid structural models. All nodes have extra outputs: accelerations in X-, Y- and Z-direction. From these the velocity and translation can be derived. In the simulations the elements are assumed to have bilinear material properties.

COMBIN14

The COMBIN14 element is a 1D, 2D or 3D spring and damper element. It can be used in two variants: axial or torsional. The two attached nodes, I and J in figure A2, have the X-, Y- and Z-directional translation as degree of freedom for the axial variant. Rotations are calculated in the torsional variant instead of translations. In the axial variant tension-compression state bending and torsion are not considered, whereas in the torsional variant bending and axial loads are not considered. The element can be combined with mass elements. Material properties such as stiffness K or damping ratio C are defined using the real constants. These elements can be stacked, meaning multiple elements using the same two nodes (I and J in figure A2). Two elements with stiffness K will produce the same result as one element with stiffness 2*K. This is useful when converting to the explicit model that uses the COMBI165 element.

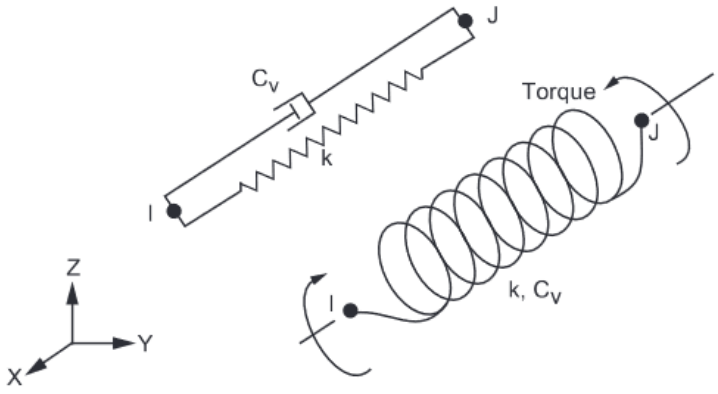

Figure A.2: Two possible variants of COMBIN14 element

COMBI165

This is the explicit version of COMBIN14. Although the main idea is the same, this element can only be used to model one thing at a time: spring or damper. This element can be stacked as well. In this thesis in the implicit simulation the COMBIN14 element modelled both a spring and a damper, and this results in two COMBIN165 elements needed in the explicit simulations

BEAM4

The BEAM4 element is most suitable for analysis of slender beam-like structures. It is based on Timoshenko theory and thus includes shear effect, but also optional (un)restrained warping effects. It is a linear, quadratic of cubic element with 6 or 7 degrees of freedom per node. These degrees of freedom are the translation and rotation in and around the three directions (X, Y, Z) and optional warping. This element is well suited for simulations involving large rotations and non-linearities.
In this thesis this element is used in the axle. Via a few of these elements the torque is transferred to the wheel, causing the wheel to rotate.

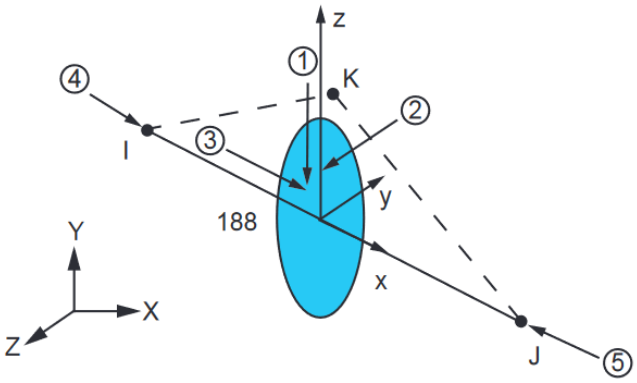

Figure A.3: Beam element

CONTA174 & TARGE170

CONTA and TARGE-elements are used to define the contact areas in the model, which do not need to be in contact from the start. If contact between bodies is not defined, the software does not know that there should be no penetration of the bodies. See appendix B for the contact calculations. These elements are placed on the outside of the selected bodies and overlay the area defined for contact. The bodies can be a solid, a shell or a line. Both CONTA and TARGE-elements share the boundary conditions with bodied they are attached to. With a deformable body they will deform with it, without influencing that deformation.

These specific elements, the 174- and 170-type, are specifically designed for 3D solid objects in contact. Not only the normal load is calculated, also frictional and tangential forces are calculated. The TARGE-element is the more stationary body which defines the 'master' nodes, in this case the rail surface. The CONTA-element is used for the wheel surface, the 'slave' nodes. For this thesis, the surface-to-surface contact definition is used. Targe170 is drawn in fig A.4 as triangular shape but can take the shape of the elements used to generate its assigned body. In the simulations in this thesis that is the surface of a hexahedral element, which is a quadrilateral.

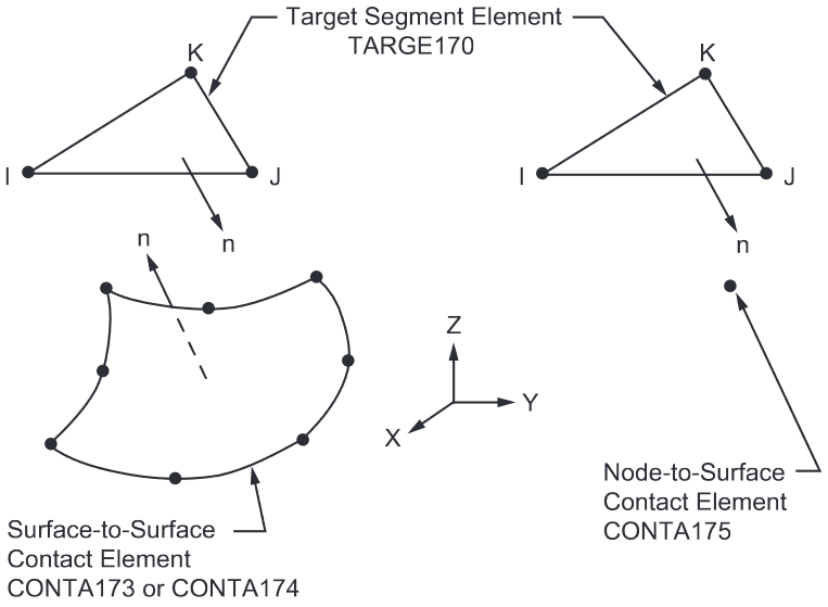

Figure A.4: Contact defined via TARGE170 and CONTA174 elements

Appendix B: Contact theory in FEM

In any FE-model the contact between certain areas or bodies should be defined. There are a couple of principles which can be used to calculate the contact pressures. The most widely used are the *Pure Penalty Method* and *Augmented Lagrange Method*. Both these methods are so-called 'penalty methods', which means that the nodes of the moving body (Slave-nodes) move into the other body (Master-nodes). A spring is imagined between the slave and master nodes, which enables the calculations of a force that would be needed to prevent penetration.

Ideally the penetration is zero, but this cannot be achieved. The stiffness of the spring can be altered to get an accurate solution with negligible penetration. The *Augmented Lagrange Method* assumes a small penetration is always present, making it less sensitive to the selected stiffness. This small penetration which is present is an error margin and ensures less iterations have to be performed, resulting is faster simulations.

In figure B1 the principle of a penetration method is presented. The green nodes displace down. The dept of the penetration is found using the locations of the defined contact nodes. With this distance and the imagined spring between them a force is assumed on the node to separate them and prevent the penetration. These calculations are iterative and go on until there is no penetration or a certain threshold is reached.

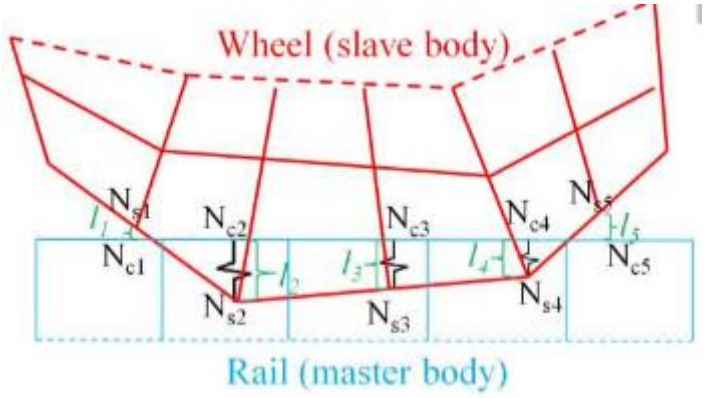

Figure B.1: Theory of contact calculations (Yang et al., 2018)